Amplitude Analysis of Charge-Exchange and Strangeness-Exchange Processes in Pseudoscalar-Meson-Baryon Scattering Using the Dual Absorptive Model*

J. S. Loos and J. A. J. Matthews
Stanford Linear Accelerator Center, Stanford University, Stanford, California 94305
(Received 10 July 1972)

An amplitude analysis of charge-exchange and strangeness-exchange reactions in pseudoscalar-meson–baryon scattering is presented for the momentum interval ~4 to ~16 GeV/c. The imaginary parts of the s-channel helicity-nonflip and helicity-flip amplitudes are assumed to have "J_0" and "J_1" structures, respectively, as specified by the dual absorptive model of Harari. This model has been successful previously in explaining the main features of elastic scattering data. The present analysis applies this model to inelastic scattering reactions and determines empirically the real part of the s-channel nonflip amplitude from the data. The resulting amplitudes reproduce well the existing differential cross section and polarization data for charge-exchange and strangeness-exchange reactions. The ρ and A_2 amplitudes in KN charge exchange are found to be in approximate agreement with strong exchange degeneracy. In contrast, the K^* and K^{**} amplitudes in Σ and Λ reactions are not strongly exchange-degenerate, even though equal forward differential cross sections are observed for the line-reversed pairs of reactions $\pi N \to KY$ and $\bar{K}N \to \pi Y$.

I. INTRODUCTION

Many studies of charge-exchange and strangeness-exchange data have been made using simple Regge poles,[1] SU(2) or SU(3) relations,[2,3] FESR (finite-energy sum rules),[4,5] complex Regge poles,[6] Regge models with absorption or cuts,[7-17] and direct amplitude analyses of the data.[18-22] The main conclusions are:

(1) Simple Regge-pole models using only leading Regge exchanges cannot describe the data.

(2) The helicity-flip amplitudes are found to have the simple Regge-pole form, with absorption (cuts) playing a minor role.

(3) The helicity-nonflip amplitudes do not have a simple Regge-pole form but appear to be significantly affected by absorption.

(4) It is not clear how absorption effects are to be calculated.

Evidence for the importance of absorption has recently been reemphasized by Harari.[23] In particular, Harari observed that the "crossover" effect in elastic scattering occurs at approximately the same value of momentum transfer, $-t \sim 0.2$ GeV^2, as the zeros in the contributions of the prominent πN resonances to the nonflip scattering amplitude at low energy.[24,25] Simple Regge-pole models would have predicted the first zero of the nonflip amplitude to occur at $-t \sim 0.6$ GeV^2. Harari then obtains a consistent interpretation of the data by assuming that duality[24,26,27] relates s-channel resonance structure to absorbed Regge-exchange amplitudes.

The subsequent introduction of the dual absorptive model (DAM) by Harari[25,28] has explained the features of elastic scattering differential cross sections and polarizations that had previously eluded the weak[12,13] and strong[11] absorption models. In the DAM, the imaginary part of the Regge-exchange s-channel helicity-nonflip amplitude is assumed to have an approximate "J_0" behavior with an absorption zero at $-t \simeq 0.2$ GeV^2 ("crossover" zero). The extractions of this amplitude from the data, both for crossing-odd (ρ, ω^0) (Refs. 29 and 30) and -even (f^0) (Ref. 31) Regge exchanges, have proven to be in good agreement with this prediction. The helicity-flip amplitudes in the DAM are expected to be nearly Regge-like, in agreement with elastic polarization data and the differential cross sections for $\pi^- p \to \pi^0 n$ and $\pi^- p \to \eta^0 n$.

Despite these successes the DAM provides no simple prediction for the real part of the s-channel helicity-nonflip amplitude. Apart from πN scattering,[18] little is known about this component of the scattering amplitude. In the present analysis we empirically determine this amplitude, and simultaneously obtain a comparison of the DAM to the reactions

$$\pi^- p \to \pi^0 n, \tag{1}$$

$$\pi^- p \to \eta^0 n, \tag{2}$$

$$K_L^0 p \to K_S^0 p, \tag{3}$$

and to the pairs of s-u crossed reactions

$$K^+ n \to K^0 p, \tag{4a}$$

$$K^- p \to \bar{K}^0 n, \tag{4b}$$

$$K^- p \to \pi^- \Sigma^+, \tag{5a}$$

$$\pi^+ p \to K^+ \Sigma^+, \tag{5b}$$

$$\bar{K}^0 p \to \pi^+ \Lambda^0, \tag{6a}$$

$$\pi^- p \to K^0 \Lambda^0. \tag{6b}$$

The purpose of our analysis is to investigate whether a consistent and simple description of the above reactions can be found in the momentum-transfer interval, $0 \leq -t \leq 1$ GeV^2, and in the momentum interval from ~4 to ~18 GeV/c. The scattering amplitudes are determined for each of the above reactions. Processes related by s-u crossing are then compared in a manner that explicitly includes the effects of absorption. Tests of exchange degeneracy[32] are possible, therefore, without having to rely on the predictions of simple Regge models implicit in previous comparisons.[33,34]

We have also compiled the strangeness-exchange data for reactions (5) and (6) in the momentum interval ~3 to ~16 GeV/c. Certain general features of the data are noted to have direct implications on the structure of the helicity amplitudes. These systematics of the data are compared to the results of the DAM, and to the predictions of Regge-pole and Regge-absorption models.

II. PARAMETRIZATION OF THE DUAL ABSORPTIVE MODEL

The dual absorptive model has been previously described by Harari.[25,28] The features of this model are largely extracted from the data and include in a direct manner the effects of absorption.[35]

The s-channel helicity amplitudes initially suggested by Harari have the following forms:

$$\begin{aligned}
&\mathrm{Im}M_{\Delta\lambda=0}(s,t) \propto (\pm)\text{“}J_0(r\sqrt{-t})\text{”} \begin{pmatrix}\text{vector}\\ \text{tensor}\end{pmatrix},\\
&\mathrm{Re}M_{\Delta\lambda=0}(s,t) \propto \text{unknown},\\
&\mathrm{Im}M_{\Delta\lambda=1}(s,t) \propto (\pm)\text{“}J_1(r\sqrt{-t})\text{”} \begin{pmatrix}\text{vector}\\ \text{tensor}\end{pmatrix},\\
&\mathrm{Re}M_{\Delta\lambda=1}(s,t) \propto \text{“}J_1(r\sqrt{-t})\text{”}\tan[\tfrac{1}{2}\pi\alpha(t)] \quad \text{(vector exchange)}\\
&\qquad\qquad \propto \text{“}J_1(r\sqrt{-t})\text{”}\cot[\tfrac{1}{2}\pi\alpha(t)] \quad \text{(tensor exchange)},
\end{aligned} \tag{7}$$

where $\Delta\lambda$ is the net change in s-channel helicity, $\alpha(t)$ is the Regge trajectory function, and r is the "interaction radius." "$J_{\Delta\lambda}$" is a Bessel function appropriately corrected for contributions to the scattering amplitude coming from a finite interval in impact-parameter space; a typical parametrization[25,28] is of the form

$$\text{“}J_{\Delta\lambda}(r\sqrt{-t})\text{”} \approx e^{At} J_{\Delta\lambda}(r\sqrt{-t}).$$

To make a more quantitative comparison of the model to the data, we choose the following parametrization for the s-channel nonflip amplitudes:

$$\begin{aligned}
&\mathrm{Im}M^V_{\Delta\lambda=0}(s,t) = g_0^V (s/s_0)^{\alpha(t)} e^{A_V t'} J_0(r\sqrt{-t'}),\\
&\mathrm{Re}M^V_{\Delta\lambda=0}(s,t) = g_0^V (s/s_0)^{\alpha(t)} e^{A_V t'} \times (1 + a_V t' + b_V t'^2 + c_V t'^3)\\
&\qquad\qquad \times e^{B_V t'} \tan[\tfrac{1}{2}\pi\alpha(0)],
\end{aligned} \tag{8a}$$

for vector exchanges; and for tensor exchanges:

$$\begin{aligned}
&\mathrm{Im}M^T_{\Delta\lambda=0}(s,t) = -g_0^T (s/s_0)^{\alpha(t)} e^{A_T t'} J_0(r\sqrt{-t'}),\\
&\mathrm{Re}M^T_{\Delta\lambda=0}(s,t) = g_0^T (s/s_0)^{\alpha(t)} e^{A_T t'} \times (1 + a_T t' + b_T t'^2) e^{B_T t'}\\
&\qquad\qquad \times \cot[\tfrac{1}{2}\pi\alpha(0)],
\end{aligned} \tag{8b}$$

where the real parts of the amplitudes have been parametrized by polynomials in $t' = t - t_{\min}$,[36] and where the Regge phase is assumed to hold for $t = 0$. This phase choice is in agreement with data on K^0_S regeneration[37] and with the determination of the forward πN charge-exchange amplitudes in Ref. 22.

The helicity-flip amplitudes have been chosen similarly:

$$\begin{aligned}
&M^V_{\Delta\lambda=1}(s,t) = g_1^V (s/s_0)^{\alpha(t)} \text{“}J_1^V(r\sqrt{-t'})\text{”} \times \{\tan[\tfrac{1}{2}\pi\alpha(t)] + i\},\\
&M^T_{\Delta\lambda=1}(s,t) = g_1^T (s/s_0)^{\alpha(t)} \text{“}J_1^T(r\sqrt{-t'})\text{”} \times \{\cot[\tfrac{1}{2}\pi\alpha(t)] - i\}.
\end{aligned} \tag{9}$$

To remove the difficulties of Eq. (9) that occur when the zeros of the Bessel function and the singularities for integer values of $\alpha(t)$ do not precisely coincide, the functions "J_1" for vector- and tensor-exchanges have been chosen as follows:

$$\begin{aligned}
&\text{“}J_1^V(r\sqrt{-t'})\text{”} \equiv J_1(r\sqrt{-t'}) e^{A_V t'} \times \left(\frac{\cos[\tfrac{1}{2}\pi\alpha(t)]\cos[\tfrac{1}{2}\pi\beta(0)]}{\cos[\tfrac{1}{2}\pi\beta(t')]\cos[\tfrac{1}{2}\pi\alpha(0)]}\right),\\
&\text{and}\\
&\text{“}J_1^T(r\sqrt{-t'})\text{”} \equiv J_1(r\sqrt{-t'}) e^{A_T t'} \times \left(\frac{\sin[\tfrac{1}{2}\pi\alpha(t)]\sin[\tfrac{1}{2}\pi\beta(0)]}{\sin[\tfrac{1}{2}\pi\beta(t')]\sin[\tfrac{1}{2}\pi\alpha(0)]}\right).
\end{aligned} \tag{10}$$

We note that the r and A parameters in Eqs. (8) and (10) are chosen to be independent of helicity; this restriction is consistent with preliminary fits to the data which allowed the r and A parameters to be different for the two helicity amplitudes. The function $\beta(t')$ is defined to be zero and minus one at the first and second zeros of $J_1(r\sqrt{-t'})$, respectively:

$$\beta(t') = \beta_0 + \beta_1 t',$$
$$\beta_0 = X_1^2/(X_2^2 - X_1^2), \qquad (11)$$
$$\beta_1 = r^2/(X_2^2 - X_1^2),$$

where X_1 (X_2) is the position of the first (second) zero of $J_1(X)$.[38] The resulting amplitudes, $M_{\Delta\lambda=1}$, are now free from singularities in the region of interest, $-t \lesssim 1$ GeV^2. To show that Eqs. (9) and (10) do provide a smooth interpolation for the real part of the tensor helicity-flip amplitude, in Fig. 1 we compare this form (solid curve) to a typical example for the singular form (dashed curve):

$$J_1(r\sqrt{-t'})e^{At'}\cot[\tfrac{1}{2}\pi\alpha(t)]\,.$$

For our fits to the data, the parameters in Eqs. (8) and (9) are: the coupling constants, $g_{\Delta\lambda}$; the exponential slope parameters A and B; the polynomial coefficients a, b, and c; and the interaction radius r. The amplitudes have been defined to have the explicit energy dependence of Regge theory; $\alpha(t)$ is the "ρ" trajectory, $\alpha(t) = 0.5 + 0.9t$, and s_0 is set equal to 1 GeV^2. The model parameters are assumed to be independent of energy over the energy region studied.[39] These choices are suggested by the absence of an appreciable energy dependence in the polarization for the charge-exchange and strangeness-exchange data (see Figs. 3, 12, and 13), together with the shrinkage of the differential cross sections observed in the same data (see Figs. 2, 16, and 17).

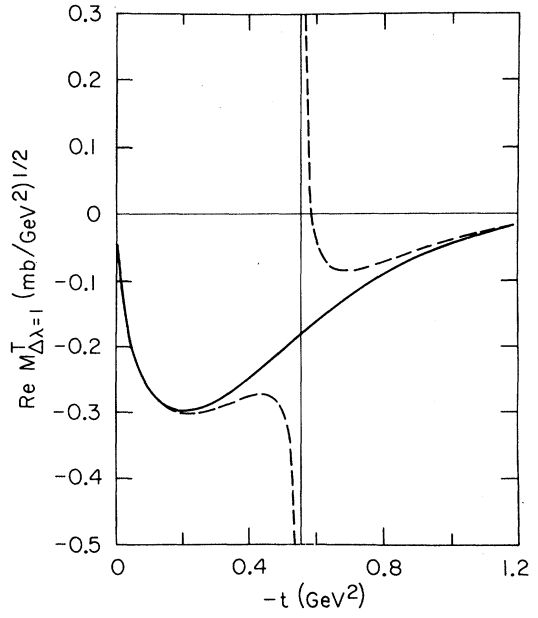

FIG. 1. Example of the real part of the helicity-flip amplitude for tensor exchange in the present formulation of the DAM (solid curve). The dashed curve is of the form

$$J_1(r\sqrt{-t'})\,e^{At'}\cot[\tfrac{1}{2}\pi\alpha(t)],$$

where a singularity (vertical line) results when the zero $\alpha(t)$ is slightly displaced from the zero in the Bessel function.

For the present analysis the differential cross section has been defined by

$$\frac{d\sigma}{dt} = \frac{(\hbar c)^2}{64\pi s q^2}\sum_{\Delta\lambda}|M_{\Delta\lambda}|^2 \text{ mb/GeV}^2, \qquad (12)$$

where q is the center-of-mass momentum.[40] Finally, the polarization, P, and T and S parameters are given by[41]

$$P = \frac{-2\,\mathrm{Im}(M_{\Delta\lambda=0}M^*_{\Delta\lambda=1})}{|M_{\Delta\lambda=0}|^2 + |M_{\Delta\lambda=1}|^2}\,,$$
$$T = \frac{-2\,\mathrm{Re}(M_{\Delta\lambda=0}M^*_{\Delta\lambda=1})}{|M_{\Delta\lambda=0}|^2 + |M_{\Delta\lambda=1}|^2}\,, \qquad (13)$$
$$S = \frac{|M_{\Delta\lambda=0}|^2 - |M_{\Delta\lambda=1}|^2}{|M_{\Delta\lambda=0}|^2 + |M_{\Delta\lambda=1}|^2}\,.$$

III. DAM COMPARISON TO THE DATA

We first compare the DAM to πN charge-exchange data to obtain a consistency check of the parametrical description of the amplitude structure described in Sec. II. Many of the features of these amplitudes have already been determined by Halzen and Michael[18] in an analysis of a complete set of πN scattering data at 6 GeV/c. Having found that the ρ-exchange amplitudes in the DAM are in agreement with previous studies, we then deal with reactions (2)–(4) which isolate ρ, ω^0, and A_2 exchanges. The analysis then turns to the K^* and K^{**} exchange reactions (5)–(6). A brief review of the experimental data indicates the importance of absorption in these channels and suggests energy trends. The K^* and K^{**} amplitudes are then determined, and compared to the ρ and A_2 amplitudes.

A. Study of ρ- and A_2-Exchange-Dominated Channels

The results of comparing the present model to the data for reactions (1) and (2) are shown in Figs. 2 and 3. The parameters determined from these data are given in Table I, and the data sources are compiled in Table II. The energy and momentum-transfer dependence of the differential cross sections and polarization are seen to be well reproduced by the model.

The corresponding amplitude structure evaluated at 6 GeV/c is shown in Fig. 4. The helicity-flip amplitudes are in agreement with simple-pole models containing nonsense-wrong-signature zeros; the nonflip amplitudes are strongly ab-

sorbed with the imaginary parts showing the "crossover" zero at $-t \sim 0.2$ GeV^2. For the η^0 amplitudes the real part of the nonflip amplitude is not well determined past $-t \gtrsim 0.2$ GeV^2 since accurate polarization data do not exist in this momentum-transfer region.[42]

The πN charge-exchange amplitudes are observed to be in good agreement with previous amplitude analyses.[18,19,21] In particular, a qualitative comparison to the results of Halzen and Michael[18] is shown in Fig. 4(a); a quantitative comparison is not possible, however, since the over-all phase of the πN amplitudes in Ref. 18 is undetermined. For the present figure the amplitudes of Halzen and Michael have been rotated by a constant phase, ~14°, to agree with the Regge phase at $t=0$.

The absorption parameters r and A determined from reactions (1) and (2) (see Table I) are observed to be in good agreement with the values found for $(\rho, \omega)^0$ and f^0 amplitudes[29-31] from analyses of the nonflip amplitudes for elastic scattering. This agreement is interesting since in the present analysis these parameters are determined from helicity-flip dominated processes. This agreement also shows the consistency of our parametrization in Eqs. (8) and (10) where we assume that r and A are independent of helicity.

If we define $A' \equiv A + \alpha' \ln(s/s_0)$, then the imagi-

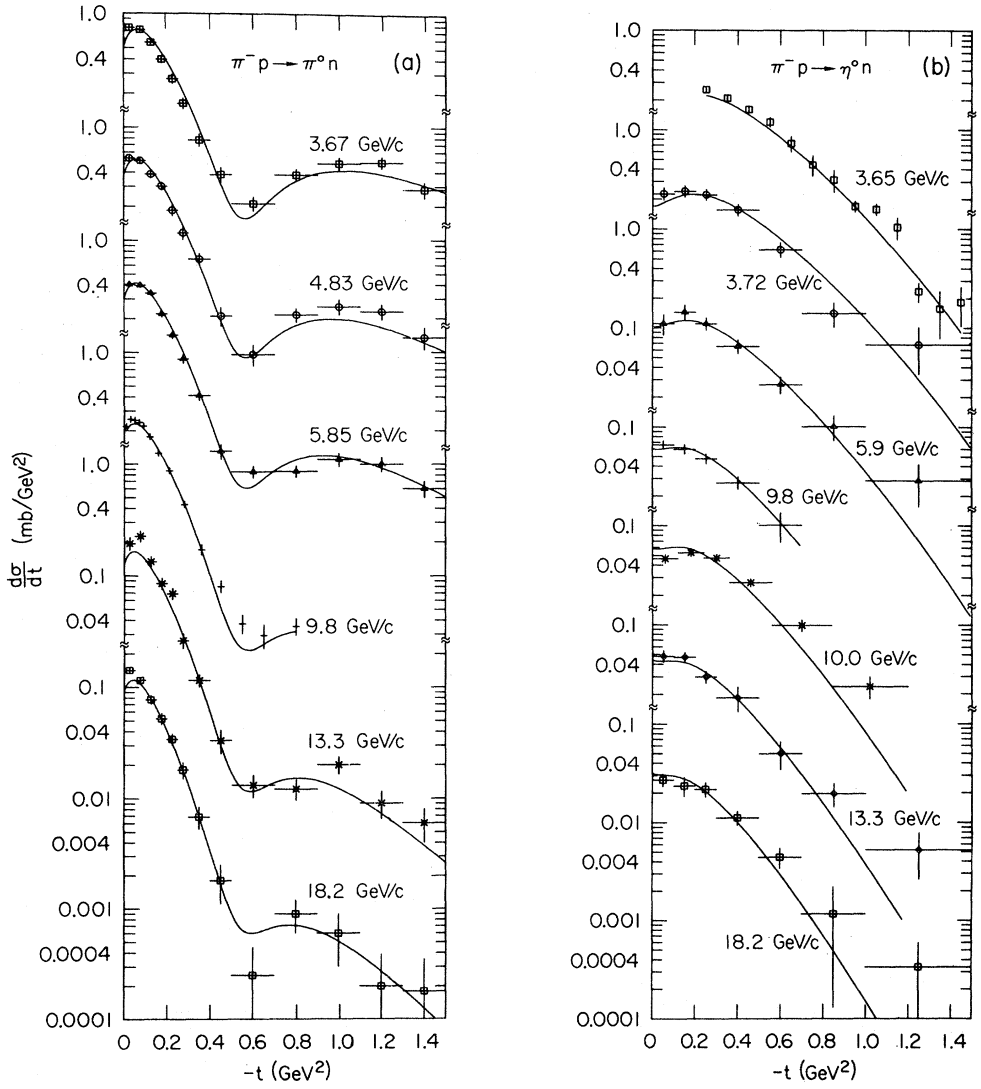

FIG. 2. Differential cross sections for (a) $\pi^- p \to \pi^0 n$ and (b) $\pi^- p \to \eta^0 n$ from references in Table II. The curves are the DAM descriptions of the data (see Sec. III A).

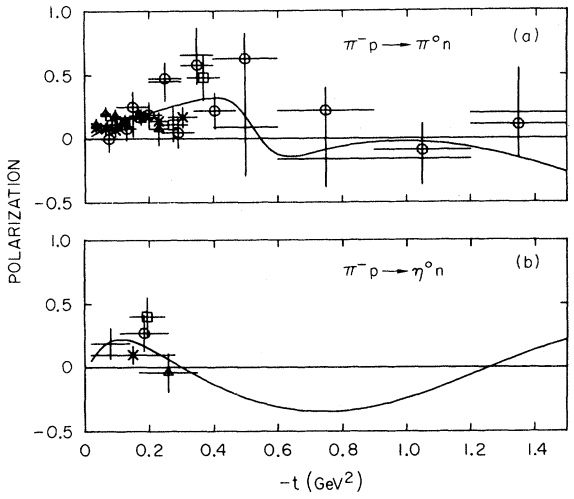

FIG. 3. Polarization data for (a) $\pi^- p \to \pi^0 n$ and (b) $\pi^- p \to \eta^0 n$ in the momentum interval 3.6–18.2 GeV/c. The curves are the DAM comparisons to the data.

nary part of the DAM amplitude is

$$\mathrm{Im}M_{\Delta\lambda}(t) = C e^{A't} J_{\Delta\lambda}(r\sqrt{-t}),$$

and the Bessel transform in impact-parameter space is[35]

$$\mathrm{Im}\tilde{M}_{\Delta\lambda}(b) = \left(\frac{C}{2A'}\right) \exp\left[-\left(\frac{r^2+b^2}{4A'}\right)\right] I_{\Delta\lambda}\left(\frac{rb}{2A'}\right), \tag{14}$$

where $I_{\Delta\lambda}$ is the hyperbolic Bessel function. For the region $(rb/2A') \gg 1$, this reduces to

$$\mathrm{Im}\tilde{M}_{\Delta\lambda}(b) \approx \frac{C}{2(\pi r b A')^{1/2}} \exp\left(\frac{-(r-b)^2}{4A'}\right) \times\left(1 - \frac{4\Delta\lambda^2 - 1}{8(rb/2A')}\right), \tag{15}$$

which is independent of $\Delta\lambda$ for sufficiently large values of $(rb/2A')$. In the region $b \sim r$ the $\Delta\lambda$ dependence is negligible for the present analysis,[43] and the amplitudes are nearly Gaussian, centered at r and with width $(2A')^{1/2}$. To the extent that Eq. (15) is independent of $\Delta\lambda$, the agreement with the results of Davier and Harari[29-31] therefore indicates that the impact-parameter representations of the helicity-flip and -nonflip amplitudes are the same.

We now consider the KN charge-exchange reactions for which the amplitudes are assumed to be linear combinations of the vector and tensor amplitudes determined from the above fits to πN charge exchange and η^0 production. Thus, in the model comparisons to the KN charge-exchange data (see Table II) only the coupling constants, and the parameters r and A are allowed to vary. The results for the differential cross section, shown in Fig. 5(a), agree well with the data. The model parameters found are presented in Table I. The predictions of SU(3) for the coupling constants (see Table III) are also given in Table I and the agreement is observed to be good.

The amplitudes for KN charge exchange are shown in Fig. 6. For the exotic K^+n channel the

TABLE I. Model parameters for reactions with ρ, ω^0, and A_2 exchanges in the t channel.

Reaction	$\pi^- p \to \pi^0 n$	$\pi^- p \to \eta^0 n$	$K^+ n \to K^0 p$ [a]	$K_L^0 p \to K_S^0 p$ Solution 1	$K_L^0 p \to K_S^0 p$ Solution 2
r (GeV^{-1})	5.19	4.99	5.13	5.00	5.13
Vector exchange	ρ	···	ρ	$\rho+\omega^0$	$\rho+\omega^0$
A_V (GeV^{-2}) [b]	−0.93	···	−1.11	−1.20	−1.95
g_0^V	−15.0	···	−10.4 (−10.6)	−15.8	−15.3
g_1^V	−30.9	···	−21.8 (−21.9)	11.9	10.7
a_V (GeV^{-2})	5.56	···	5.56	5.56	5.56
b_V (GeV^{-4})	10.20	···	10.20	10.20	10.20
c_V (GeV^{-6})	5.22	···	5.22	5.22	5.22
B_V (GeV^{-2})	1.5	···	1.5	1.5	1.5
Tensor exchange	···	A_2	A_2	···	···
A_T (GeV^{-2}) [b]	···	−0.72	−0.70	···	···
g_0^T	···	−7.56	−8.88 (−9.25)	···	···
g_1^T	···	−14.9	−16.3 (−18.2)	···	···
a_T (GeV^{-2})	···	7.28	7.28	···	···
b_T (GeV^{-4})	···	4.88	4.88	···	···
B_T (GeV^{-2})	···	2.0	2.0	···	···

[a] SU(3) predictions for the coupling constants, $g_{\Delta\lambda}$, are shown in parentheses, see Sec. III A.

[b] For comparison of the present A parameters to the exponential parameter of Harari, A' (see Ref. 29) we note that $A' = A + \alpha' \ln(s/s_0) \approx A + 2.1$ GeV^{-2} at 5 GeV/c.

TABLE II. Summary of experimental data references.

Reaction	Expt. momenta (GeV/c)	Reference
$\pi^- p \to \pi^0 n$	3.67, 4.83, 5.85, 13.3, 18.2	P. Sonderegger *et al.*, Phys. Letters 20, 75 (1966).
	9.8	A. V. Stirling *et al.*, Phys. Rev. Letters 14, 763 (1965).
	5.9, 11.2	P. Bonamy *et al.*, Phys. Letters 23, 501 (1966); P. Bonamy *et al.*, Nucl. Phys. B16, 335 (1970).
	3.47, 5.0	D. D. Drobnis *et al.*, Phys. Rev. Letters 20, 274 (1968).
	5.0, 8.0	O. Guissan, presented at Rencontre de Moriond, 1971 (unpublished).
$\pi^- p \to \eta^0 n$	3.72, 5.9, 9.8, 13.3, 18.2	O. Guissan *et al.*, Phys. Letters 18, 200 (1965).
	3.65	E. H. Harvey *et al.*, Phys. Rev. Letters 27, 885 (1971).
	10.0	M. A. Wahlig and I. Mannelli, Phys. Rev. 168, 1515 (1968).
	3.2, 3.47, 5.0	D. D. Drobnis *et al.*, Phys. Rev. Letters 20, 274 (1968).
	5.9, 11.2	P. Bonamy *et al.*, Nucl. Phys. B16, 335 (1970).
$K_L^0 p \to K_S^0 p$	2–4, 4–8	A. D. Brody *et al.*, Phys. Rev. Letters 26, 1050 (1971); SLAC Group B (private communication).
$K^- p \to \bar{K}^0 n$	5.0, 7.1, 9.5, 12.3	P. Astbury *et al.*, Phys. Letters 23, 396 (1966).
$K^+ n \to K^0 p$	5.5	D. Cline *et al.*, Nucl. Phys. B22, 247 (1970).
	12.0	A. Firestone *et al.*, Phys. Rev. Letters 25, 958 (1970).
$\pi^+ p \to K^+ \Sigma^+$	3.0, 3.25, 4.0, 5.05, 7.0	S. M. Pruss *et al.*, Phys. Rev. Letters 23, 189 (1969).
	3.23	R. R. Kofler *et al.*, Phys. Rev. 163, 1479 (1967).
	5.4	W. A. Cooper *et al.*, Phys. Rev. Letters 20, 472 (1968).
	6.0, 10.0, 14.0	A. Bashian *et al.*, Phys. Rev. D 4, 2667 (1971).
$\pi^- p \to K^0 \Sigma^0$	2.0, 3.1, 4.0	O. I. Dahl *et al.*, Phys. Rev. 163, 1430 (1967).
$\to K^0 \Lambda^0$	3, 4, 5, 6	C. E. W. Ward *et al.*, Bull. Am. Phys. Soc. 17, 126 (1972); C. E. W. Ward (private communication).
	3.9	M. Abramovich *et al.*, Nucl. Phys. B27, 477 (1971).
	4.5, 6.0	D. J. Crennell *et al.*, Phys. Rev. D 6, 1220 (1972).
	7.91	R. Ehrlich *et al.*, Phys. Rev. 152, 1194 (1966).
	8.0, 10.7, 15.7	W. H. Willen *et al.*, in Proceedings of the Fourth International Conference on High Energy Collisions, Oxford, 1972 (unpublished); W. A. Love (private communication).
$\pi^+ n \to K^+ \Lambda^0$	6.95	J. Lynch (private communication).
$K^- p \to \pi^- \Sigma^+$	3.95	L. Moscoso *et al.*, Nucl. Phys. B36, 332 (1972).
	4.07, 5.47	J. S. Loos *et al.*, Phys. Rev. 173, 1330 (1968).
	8.0, 16.0	D. Birnbaum *et al.*, Phys. Letters 31B, 484 (1970).
$K^- n \to \pi^- \Sigma^0$	3.0	S.A.B.R.E. Collaboration, Nucl. Phys. B33, 61 (1971).
$\to \pi^- \Lambda^0$	3.6, 3.9	D. J. Crennell *et al.*, Phys. Rev. Letters 23, 1347 (1969).
	4.5	W. L. Yen *et al.*, Phys. Rev. Letters 22, 963 (1969); W. L. Yen *et al.*, Phys. Rev. 188, 2011 (1969).
	4.9	B. J. Burdick *et al.*, Nucl. Phys. B41, 45 (1972).
$\bar{K}^0 p \to \pi^+ \Sigma^0$	2–3, 3–5	A. D. Brody *et al.*, SLAC Report No. SLAC-PUB-823, 1970 (unpublished);
$\to \pi^+ \Lambda^0$	5–8	R. J. Yamartino *et al.*, Bull. Am. Phys. Soc. 17, 145 (1972); R. J. Yamartino (private communication).
$K^- p \to \pi^0 \Lambda^0$	3.5	B.G.L.O.R. Collaboration, Phys. Rev. 152, 1148 (1966).
	3.9, 4.6	M. Aguilar-Benitez *et al.*, Phys. Rev. D 6, 29 (1972).
	3.95	L. Moscoso *et al.*, (see reaction $K^- p \to \pi^- \Sigma^+$ above).
	4.1, 5.5	D. Reeder (private communication).

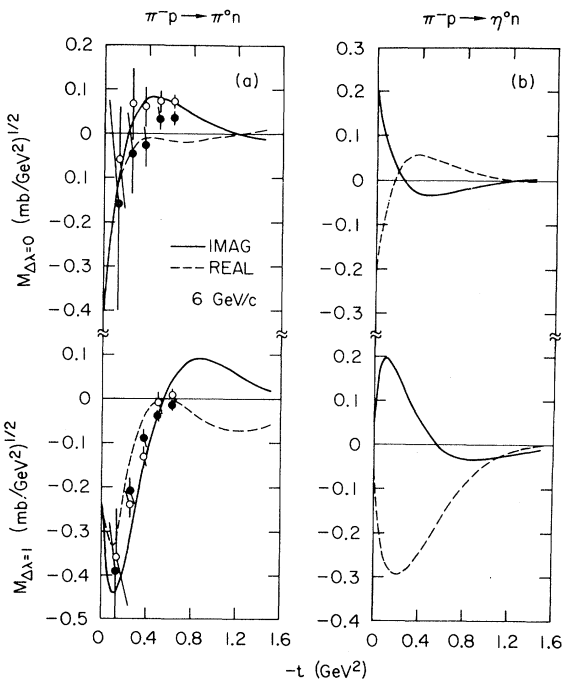

FIG. 4. s-channel helicity amplitudes evaluated at 6 GeV/c for (a) $\pi^-p \to \pi^0 n$ and (b) $\pi^-p \to \eta^0 n$. The solid (dashed) curves represent the imaginary (real) parts of the amplitudes. The imaginary parts of the amplitudes are essentially Bessel functions, $J_{\Delta\lambda}$ (see Secs. II and III A). The solid (open) points in (a) are the results of the amplitude analysis of Halzen and Michael (Ref. 18) for the real (imaginary) parts of the s-channel amplitudes. For comparisons to the present amplitudes, the amplitudes of Halzen and Michael have been rotated by a constant phase, $\sim 14°$, to agree with the Regge phase at $t=0$ (see Sec. III A).

amplitudes are seen to be predominantly real, and are in approximate agreement with the prediction of strong exchange degeneracy.[32] At $t=0$, the ratio of $\mathrm{Im}M_{\Delta\lambda=0}/\mathrm{Re}M_{\Delta\lambda=0} \simeq 10\%$ in agreement with experimental estimates using the optical theorem.[44] Since the imaginary parts of the DAM amplitudes have the same structure in t for vector and tensor exchanges, a cancellation of the imaginary terms is possible even for the strongly absorbed nonflip amplitudes.

The values for the quantities P, S, and T that result from the present parametrization are shown in Figs. 5(b)–5(d). Due to the uncertainties in $\mathrm{Re}M^T_{\Delta\lambda=0}$ mentioned previously, these predictions must be considered to be qualitative. They do suggest, however, that the polarization for K^+n will be small, that the polarization for K^-p will be negative in the interval $0.4 \lesssim -t \lesssim 1.0$ GeV^2, and that the S and T parameters will be quite similar for K^+n and K^-p channels for $-t \lesssim 0.5$ GeV^2.

The analysis of Martin, Michael, and Phillips[2] using SU(3) to relate experimental data on charge- and strangeness-exchange reactions yields a similar prediction for K^-p polarization, but suggests that the K^+n polarization will be substantially larger than that shown in Fig. 5(b). This would imply that the K^+n amplitudes possess significant imaginary parts, which is not in agreement with the present determination of the amplitude structure (see Fig. 6).

The amplitudes determined from πN charge exchange have also been compared to the data on the reaction $K^0_L p \to K^0_S p$. As in the study of KN charge exchange the model amplitudes have been constrained to the πN charge-exchange results, with only the coupling constants being allowed to change significantly. The results of this comparison, solution 1, are shown as the dashed lines in Fig. 7(a), and the parameters are recorded in Table I. Solution 1 is observed to provide a good description of the differential cross section in the region $-t \lesssim 0.3$ GeV^2, but for larger momentum transfers provides values that are too low.

An alternate solution, solution 2, is also shown in Fig. 7(a) and recorded in Table I. In this parametrization, the exponential parameter, A, has been varied to provide the best description of the $K^0_L p \to K^0_S p$ data. The resulting value, $A=-1.95$ GeV^{-2}, is significantly different, however, from the previous results for πN charge exchange and η^0 production.

We note that the imaginary part of the nonflip amplitude is the dominant term for the reaction $K^0_L p \to K^0_S p$ as expected if it proceeds mainly by ω^0 exchange.[45] The zero in this term for $-t \sim 0.2$ GeV^2 (the crossover zero) produces a steep forward peak (slope parameter ~ 10 GeV^{-2}), and in addition tends to cause a dip in the differential cross section. However, the helicity-flip amplitude does contribute in the vicinity $-t \sim 0.2$ GeV^2 such that the differential cross section exhibits a shoulder rather than a dip in this momentum-transfer region.

The polarization predictions are shown in Fig. 7(b) and suggest that the $K^0_L p \to K^0_S p$ polarization will be negative for momentum transfers $-t \lesssim 0.6$ GeV^2. The SU(3) f/d ratios for the vector nonet, given in Table IV, have been determined by comparing the coupling constants for the reactions $K^0_L p \to K^0_S p$ and $\pi^-p \to \pi^0 n$. Solutions 1 and 2 are observed to give essentially equal values of $(f/d)_{\Delta\lambda=0} \sim -5.3$ (see also Ref. 37) and $(f/d)_{\Delta\lambda=1} \sim 0.32$ for nonflip and flip coupling, respectively.

B. Study of K^* and K^{**} Exchange Reactions

To investigate systematic trends in the $\pi N \to K(\Lambda, \Sigma)$ and $\bar{K}N \to \pi(\Lambda, \Sigma)$ data and to study the

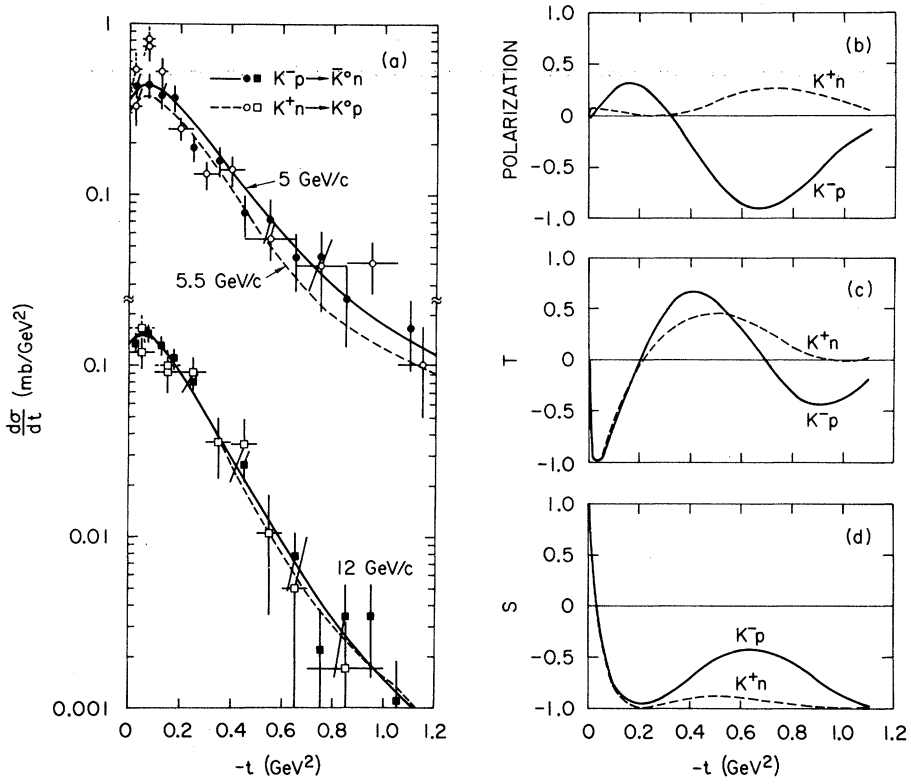

FIG. 5. (a) Comparison of KN charge-exchange differential cross sections: $K^+n \to K^0p$ at 5.5 and 12.0 GeV/c; $K^-p \to \bar{K}^0p$ at 5.0 and 12.3 GeV/c. The solid (dashed) curves are the results of DAM comparisons to the $K^-p \to \bar{K}^0n$ ($K^+n \to K^0p$) data. (b), (c), and (d) DAM predictions for KN charge-exchange polarization, T, and S parameters, respectively.

TABLE III. SU(3) relations for pseudoscalar-meson–baryon scattering.

SU(3) amplitude [a]	t-channel exchange	Reaction amplitude
A_V	ρ	$-\sqrt{\frac{1}{2}}\,A(\pi^-p \to \pi^0n)$
A_T	A_2	$\sqrt{\frac{3}{2}}\,A(\pi^-p \to \eta^0n)$
$A_V + A_T$	ρ, A_2	$A(K^-p \to \bar{K}^0n)$
$-A_V + A_T$	ρ, A_2	$A(K^+n \to K^0p)$
$(1-2\alpha)A_V$	ρ, ω^0	$-A(K_L^0p \to K_S^0p)$
$(1-2\alpha)A_V + (1-2\alpha')A_T$ [b]	K^*, K^{**}	$-A(\pi^+p \to K^+\Sigma^+) = -\sqrt{2}\,A(\pi^-p \to K^0\Sigma^0)$
$-(1-2\alpha)A_V + (1-2\alpha')A_T$ [b]	K^*, K^{**}	$-A(K^-p \to \pi^-\Sigma^+) = \sqrt{2}\,A(K^-n \to \pi^0\Sigma^-)$
		$= -\sqrt{2}\,A(K^-n \to \pi^-\Sigma^0)$
		$= -\sqrt{2}\,A(\bar{K}^0p \to \pi^+\Sigma^0)$
$(1-2\alpha/3)A_V + (1-2\alpha'/3)A_T$	K^*, K^{**}	$-\sqrt{\frac{2}{3}}\,A(\pi^-p \to K^0\Lambda^0) = -\sqrt{\frac{2}{3}}\,A(\pi^+n \to K^+\Lambda^0)$
$-(1-2\alpha/3)A_V + (1-2\alpha'/3)A_T$	K^*, K^{**}	$-\sqrt{\frac{2}{3}}\,A(\bar{K}^0p \to \pi^+\Lambda^0) = -\sqrt{\frac{2}{3}}\,A(K^-n \to \pi^-\Lambda^0)$
		$= -(2/\sqrt{3})A(K^-p \to \pi^0\Lambda^0)$

[a] The f/d ratios are contained in $\alpha \equiv 1/(f/d+1)$.

[b] The Σ amplitudes have been written assuming t-channel exchanges with isospin $\frac{3}{2}$ can be neglected.

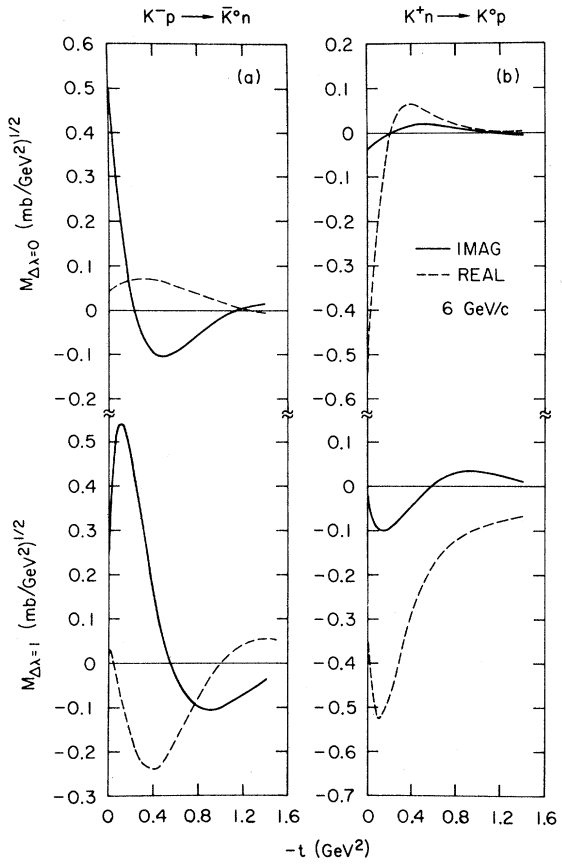

FIG. 6. Resultant s-channel helicity amplitudes, summed over ρ and A_2 exhcnages, for the reactions (a) $K^-p \to \bar{K}^0 n$ and (b) $K^+n \to K^0 p$ at 6 GeV/c. The solid (dashed) curves represent the imaginary (real) parts of the amplitudes.

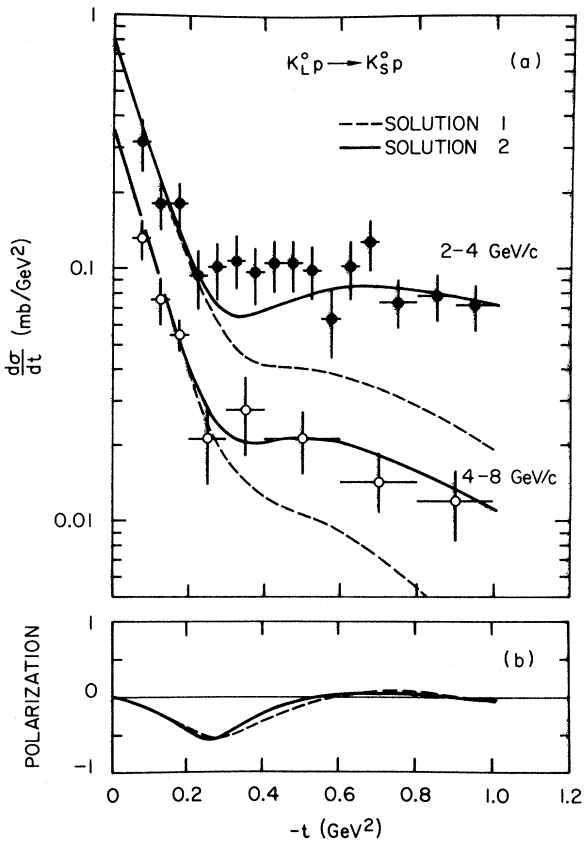

FIG. 7. (a) Differential cross sections for $K^0_L p \to K^0_S p$ in the momentum interval 2 to 8 GeV/c. The dashed (solid) curves are the results of the DAM comparison to the data for solution 1 (and 2) as discussed in Sec. III A. The corresponding polarization predictions are shown in (b).

TABLE IV. f/d ratios determined from model comparisons to the data.

Reactions	Vector exchange $(f/d)^{(V)}_{\Delta\lambda=0}$	Vector exchange $(f/d)^{(V)}_{\Delta\lambda=1}$	Tensor exchange $(f/d)^{(T)}_{\Delta\lambda=0}$	Tensor exchange $(f/d)^{(T)}_{\Delta\lambda=1}$
$\pi^-p \to \pi^0 n$ $K^0_L p \to K^0_S p$ (soln. 1)	−5.15	0.30	...	...
$\pi^-p \to \pi^0 n$ $K^0_L p \to K^0_S p$ (soln. 2)	−5.42	0.34	...	...
KN charge exchange $\bar{K}N \to \pi\Sigma$ (model 2)	−4.70	−0.45	1.78	1.35
KN charge exchange $\bar{K}N \to \pi\Lambda$ (model 2)	9.10	0.24	−0.15	−0.22
$\pi p \to K(\Lambda, \Sigma)$ $\bar{K}p \to \pi(\Lambda, \Sigma)$ (model 1)	−2.26	0.15	−2.86	0.27
$\pi p \to K(\Lambda, \Sigma)$ $Kp \to \pi(\Lambda, \Sigma)$ (model 2)	−2.11	0.15	−4.48	0.34

momentum dependence of their differential cross sections, we have made a compilation of forward differential cross sections and slopes between ~3 and ~16 GeV/c. These data,[46] from references in Table II, are shown in Figs. 8–11.

Above ~4 GeV/c, approximately equal differential cross sections at $t=0$ are observed for the Σ channels, $\pi N \to K\Sigma$ and $\bar{K}N \to \pi\Sigma$ (see Fig. 8), and also for the Λ channels, $\pi N \to K\Lambda$ and $\bar{K}N \to \pi\Lambda$ (see Fig. 10), although a nonstatistical scattering of the data points between experiments appears to be present. The slope parameters for the Σ data are nearly equal for the πN and $\bar{K}N$ channels (see Fig. 9), although the πN values appear to be slightly larger than the $\bar{K}N$ values. In contrast, the slope parameters for $\pi N \to K\Lambda$ are significantly greater than those for $\bar{K}N \to \pi\Lambda$ (see Fig. 11). The difference of slope parameters for the Λ channels has been noted previously.[33]

Regge shrinkage would predict an increase of the slopes with momentum as indicated by the curves in Figs. 9 and 11. The data are observed to be in qualitative agreement with shrinkage, but the large uncertainties cannot rule out alternate interpretations.

The measured values for the Σ and Λ polarizations are shown in Figs. 12 and 13, respectively. Two interesting trends are apparent. First, the data show no obvious change with energy, suggesting that the energy dependences of the helicity-flip and -nonflip amplitudes are the same (as expected, for example, by Regge theory). Second, the polarizations approximately obey the relations

$$P(\pi N \to K\Lambda) = -P(\pi N \to K\Sigma)$$

and

$$P(\bar{K}N \to \pi\Lambda) = -P(\bar{K}N \to \pi\Sigma).$$

This mirror symmetry suggests that the Λ and Σ channels have qualitatively similar amplitude structure and places a restriction on the relative signs of the helicity-flip and -nonflip amplitudes.[47]

It is interesting to briefly examine whether standard Regge-exchange models can account for the observed trends in the strangeness-exchange reactions. Both Λ and Σ production are assumed to be described by K^* and K^{**} Regge exchanges in the t channel.[48] Simple Regge-pole models with exchange-degenerate K^* and K^{**} trajectories

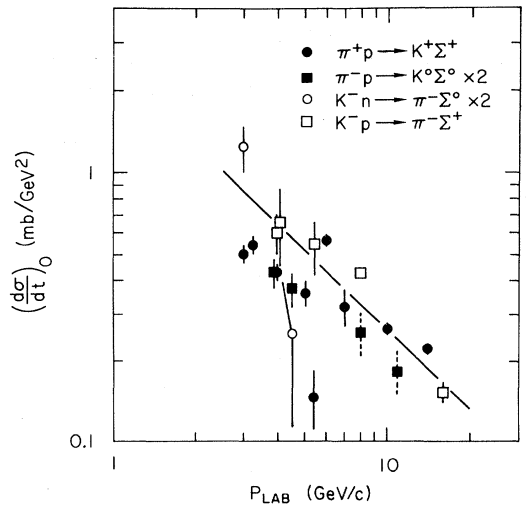

FIG. 8. Differential cross sections extrapolated to $t=0$ for $\pi N \to K\Sigma$ (solid points) and $\bar{K}n \to \pi\Sigma$ (open points). Preliminary data have dashed error bars. The data references are summarized in Table II. The curve is the comparison of the DAM to the data (see Sec. III B).

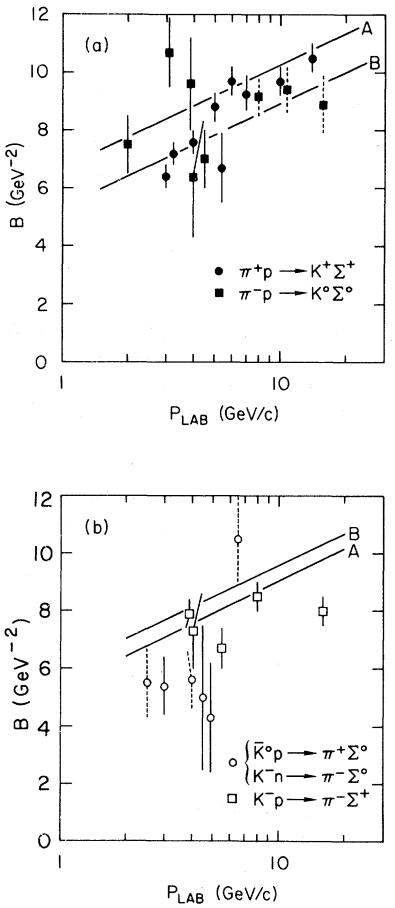

FIG. 9. Slopes of the forward differential cross sections for (a) $\pi p \to K\Sigma$ and (b) $\bar{K}N \to \pi\Sigma$. Preliminary data have dashed error bars. The data references are summarized in Table II. The curves are the comparison of the DAM (model 2) to the data for theoretical slopes calculated in the momentum-transfer intervals. A: ($0 \leq -t \leq 0.3$ GeV^2); and B: ($0.1 \leq -t \leq 0.4$ GeV^2).

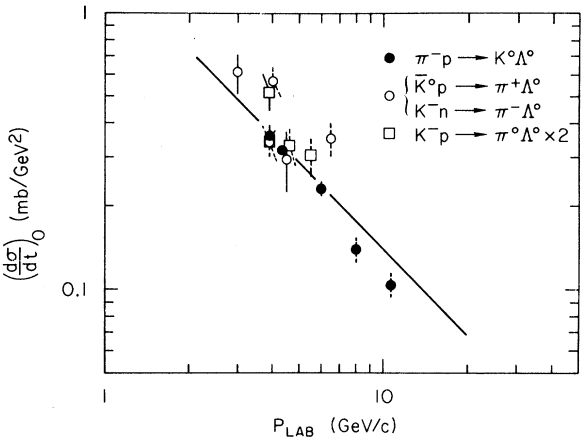

FIG. 10. Differential cross sections extrapolated to $t=0$ for $\pi N \to K\Lambda$ (solid points) and $\bar{K}N \to \pi\Lambda$ (open points). Preliminary data have dashed error bars. The data references are given in Table II. The curve is the comparison of the DAM to the data.

predict

$$\frac{d\sigma}{dt}(\bar{K}N \to \pi Y) = \frac{d\sigma}{dt}(\pi N \to KY),$$

where Y represents either Λ or Σ. This relation is observed to be approximately satisfied by all the data at $t=0$ and by the Σ data for $-t>0$, but disagrees with the Λ data away from the forward direction. Independent of exchange degeneracy, simple Regge models predict opposite signs of the polarization for $\bar{K}N$ and πN channels,

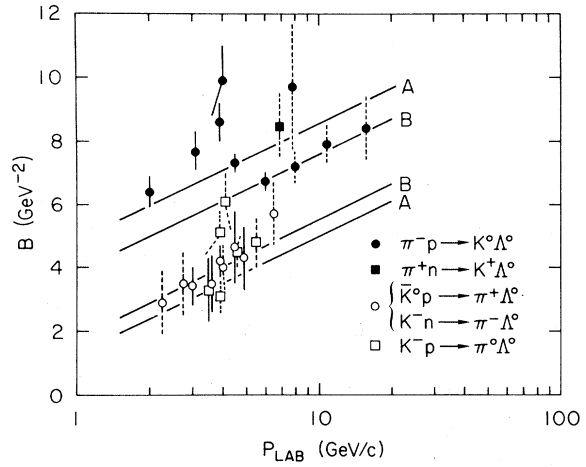

FIG. 11. Slopes of the forward differential cross sections for $\pi N \to K\Lambda$ (solid points) and $KN \to \pi\Lambda$ (open points). Preliminary data are denoted using dashed error bars. The data references are given in Table II. The solid curves are the comparison of the DAM (model 2) to the data as discussed in the caption to Fig. 9.

$$P\frac{d\sigma}{dt}(\bar{K}N \to \pi Y) = -P\frac{d\sigma}{dt}(\pi N \to KY),$$

in disagreement with the data for both Λ and Σ final states. On the other hand, standard absorption models can reproduce the experimental polarizations[14,16] but predict that

$$\frac{d\sigma/dt(\bar{K}N \to \pi Y)}{d\sigma/dt(\pi N \to KY)} < 1$$

in contradiction to observation (see Figs. 14 and 15). This result applies to both weak and strong absorption models, and arises from the subtractive nature of the absorptive corrections in these models.[14,15] In summary, no clear understanding of the reactions $\pi N \to KY$ and $\bar{K}N \to \pi Y$ is provided by the standard models.

Before making a detailed comparison of the DAM to the data, we first comment on the hypothesis of strong exchange degeneracy for the K^* and K^{**} exchanges. Since the s channel in $\bar{K}N \to \pi Y$ is not exotic, duality does not require the K^* and K^{**} exchanges to be strongly exchange-degenerate. The large polarizations observed in the $\bar{K}N$ channels, for example, disagree with strong exchange degeneracy. In contrast, the duality diagrams[26] [or equivalently, strong ex-

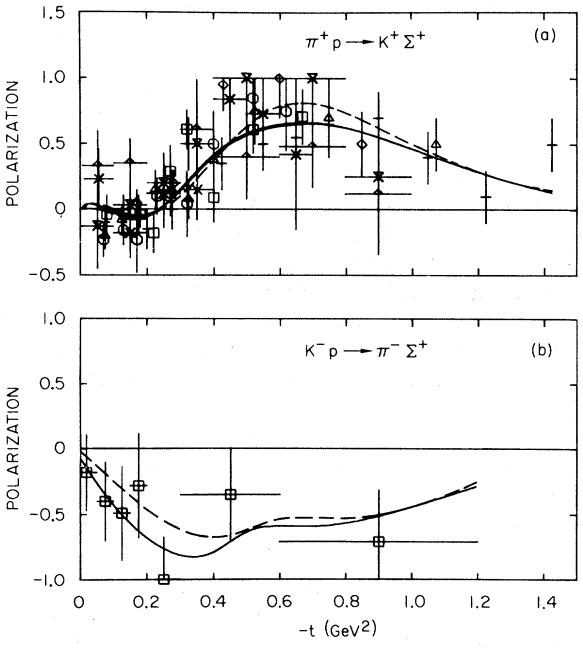

FIG. 12. Polarization for the reactions (a) $\pi^+p \to K^+\Sigma^+$ in the momentum interval 3–14 GeV/c, and (b) $K^-p \to \pi^-\Sigma^+$ at 3.95 GeV/c. The solid (dashed) curves are the comparisons of the DAM model 1 (model 2) to the data. See Sec. III B of the text for the distinction between models 1 and 2.

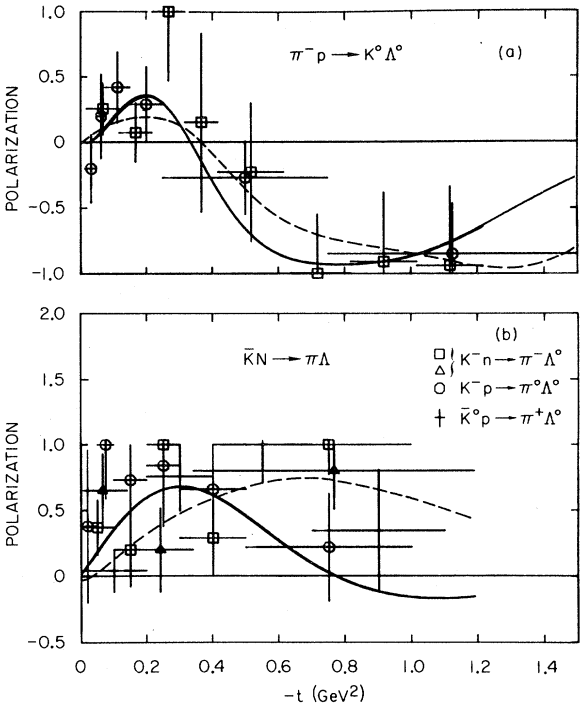

FIG. 13. Polarization for the reactions (a) $\pi^- p \to K^0 \Lambda^0$ at 3.1 and 3.9 GeV/c, and (b) $\bar{K}N \to \pi\Lambda$ in the momentum interval 3.9 to ~8 GeV/c. The solid (dashed) curves are the comparisons of the DAM model 1 (model 2) to the data.

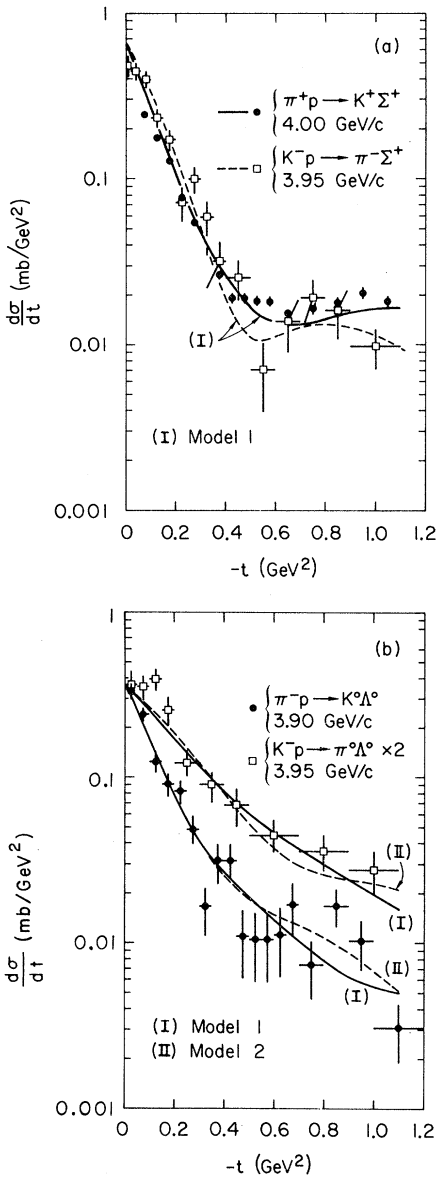

FIG. 14. Differential cross section at ~4 GeV/c for (a) $\pi^+ p \to K^+ \Sigma^+$ (solid points) and $K^- p \to \pi^- \Sigma^+$ (open points). The solid (dashed) curves, denoted (I), are the comparison of the model 1 version of the DAM to the data in the $\pi^+ p$ ($K^- p$) channel. (b) $\pi^- p \to K^0 \Lambda^0$ (solid points) and $K^- p \to \pi^0 \Lambda^0$ (open points, scaled by a factor of 2). Solid curves (I) and dashed curves (II) are the comparison of the DAM, models 1 and 2, respectively, to the data.

change degeneracy for KN charge exchange together with SU(3) symmetry and equal f/d values for vector and tensor exchanges] suggest that the amplitudes for the $\bar{K}N \to \pi Y$ channels should be purely real, and studies of the low-energy data do show an approximate averaging to zero of the imaginary part of the nonflip amplitude.[49] The present analysis using the DAM does not allow strong exchange degeneracy for the K^* and K^{**} amplitudes, however, as indicated by the following two observations:

(1) If the $\Delta\lambda = 1$ amplitudes were strongly exchange-degenerate, then the polarization for $\bar{K}N \to \pi(\Lambda, \Sigma)$ would be

$$P \propto J_0(r\sqrt{-t})\,\mathrm{Re}M_{\Delta\lambda=1}(s,t)\,.$$

The polarization would then be required to have (at least) the zero structure of $J_0(r\sqrt{-t})$; in particular it would be zero for $-t \sim 0.2$ GeV^2.[50] This feature is not observed in the present data (Figs. 12 and 13) which have polarizations in both Λ and Σ channels of ~50% in this t region. A similar argument in the region $-t \sim 0.6$ GeV^2 can be applied to the hypothesis of strong exchange degeneracy for the helicity-nonflip amplitude and is also in disagreement with the DAM.

(2) The experimental observation that

$$\frac{d\sigma/dt(\bar{K}N \to \pi Y)}{d\sigma/dt(\pi N \to KY)} > 1$$

for $-t > 0$ implies that the real parts of the vector- and tensor-exchange amplitudes are approximately

equal, rather than the imaginary parts as suggested by arguments of strong exchange degeneracy. Denoting the K^* and K^{**} amplitudes by A_V and A_T, respectively, the amplitudes for $\bar{K}N$ and πN channels are

$$A(\bar{K}N \to \pi Y) = A_V + A_T ,$$

$$A(\pi N \to KY) = -A_V + A_T .$$

The ratio $d\sigma/dt\,(\bar{K}N \to \pi Y)/d\sigma/dt\,(\pi N \to KY)$ then can be greater than unity only if $\mathrm{Re}(A_V A_T^*) > 0$. Using the parametrization for the DAM of Eqs. (8) and (9), we have

$$\mathrm{Re}(A_V A_T^*) \propto [(1 + a_V t' + b_V t'^2)(1 + a_T t' + b_T t'^2) e^{(B_V + B_T)t'}] - [J_0(r\sqrt{-t'})]^2 , \tag{16}$$

where the first (second) term is from the real (imaginary) parts of A_V and A_T. Note that the contribution to $\mathrm{Re}(A_V A_T^*)$ from the $\Delta\lambda = 1$ amplitude is zero since these amplitudes are defined to have Regge phases in Eqs. (8) and (9). As seen in Eq. (16), the imaginary parts of the amplitude considered alone would erroneously predict

$$\frac{d\sigma/dt\,(\bar{K}N \to \pi Y)}{d\sigma/dt\,(\pi N \to KY)} < 1.$$

The real parts therefore must contribute to make this ratio greater than unity. In fact, the largest splitting of the following ratio of differential cross sections,

$$\left[\frac{d\sigma}{dt}(\bar{K}N \to \pi Y) - \frac{d\sigma}{dt}(\pi N \to KY)\right] \Big/ \left[\frac{d\sigma}{dt}(\bar{K}N \to \pi Y) + \frac{d\sigma}{dt}(\pi N \to KY)\right] ,$$

tends to occur for $\mathrm{Re}A_V = \mathrm{Re}A_T$.

We now turn to the parametrization used for the K^* and K^{**} exchange amplitudes in the DAM. The basic amplitude structure is assumed to be similar to the ρ- and A_2-exchange amplitudes of Sec. III A, but now a difficulty occurs with the choice of phases. If we use a linear Regge trajectory passing through the physical K^* and K^{**} masses then a zero in the K^* helicity-flip amplitude appears at $-t \sim 0.4$ GeV^2 which no longer coincides with the first zero of the $J_1(r\sqrt{-t})$ for $r \sim 5$ GeV^{-1} (corresponding to an interaction radius of ~1 fm). The simple Regge-pole form for the helicity-flip amplitude is therefore no longer identical to the DAM amplitudes. A second difficulty occurs with the conventional value for the Regge trajectory intercept, $\alpha_{K^*}(0) \simeq 0.33$, since this value predicts a fall with energy of the cross sections which appears to be more rapid than the data [for example, Bashian *et al.*[51] find $\alpha_{\mathrm{eff}}(0) \simeq 0.7$ for $\pi^+ p \to K^+\Sigma^+$]. In order to deal with these problems we have chosen the following modified form for the vector s-channel helicity amplitudes (hereafter called model 1):

$$\mathrm{Im}M^V_{\Delta\lambda=0}(s,t) = g_0^V (s/s_0)^{\alpha(t)+\Delta\alpha} e^{A_V t'} J_0(r\sqrt{-t'}) ,$$

$$\mathrm{Re}M^V_{\Delta\lambda=0}(s,t) = g_0^V (s/s_0)^{\alpha(t)+\Delta\alpha} e^{A_V t'} (1 + a_V t' + b_V t'^2) e^{B_V t'} \tan[\tfrac{1}{2}\pi\alpha_V(0)] ,$$

and (17)

$$M^V_{\Delta\lambda=1}(s,t) = g_1^V (s/s_0)^{\alpha(t)+\Delta\alpha} e^{A_V t'} \left(J_1(r\sqrt{-t'})\, \frac{\cos[\tfrac{1}{2}\pi\alpha(t)]\cos[\tfrac{1}{2}\pi\beta(0)]}{\cos[\tfrac{1}{2}\pi\beta(t')]\cos[\tfrac{1}{2}\pi\alpha(0)]}\right)\left(\tan[\tfrac{1}{2}\pi\alpha_V(0)\, \frac{\tan[\tfrac{1}{2}\pi\alpha(t)]}{\tan[\tfrac{1}{2}\pi\alpha(0)]} + i\right),$$

where $\alpha(t)$ and $\alpha_V(t)$ are the ρ and K^* Regge trajectories, respectively, and $\Delta\alpha$ is an additional parameter used to obtain an adequate energy dependence.[52] The modifications are designed to preserve the "$J_{\Delta\lambda}$" structure while allowing the amplitudes to have the K^* Regge phase at $t = 0$. Analogous amplitudes apply for the K^{**} (tensor) exchange.

We have also considered a second parametrization, hereafter called model 2, that partially relaxes the restrictions of model 1 (Eq. 17). For model 2 the real part of the vector helicity-flip amplitude is chosen to be

$$\mathrm{Re}M^V_{\Delta\lambda=1}(s,t) = g_1^V (s/s_0)^{\alpha(t)+\Delta\alpha} e^{A_V t'} \times (\tfrac{1}{2} r\sqrt{-t'})(1 + xt' + yt'^2) \tan[\tfrac{1}{2}\pi\alpha(0)] , \tag{18}$$

where x and y are parameters to be determined from the data. The tensor amplitudes are the same as in model 1. Note that for model 2 the $\Delta\lambda = 1$ amplitudes can also contribute to the interference term evaluated in Eq. (16).

We now present the results of our analysis for the strangeness-exchange processes. In view of the difficulties in parametrization of the K^* and

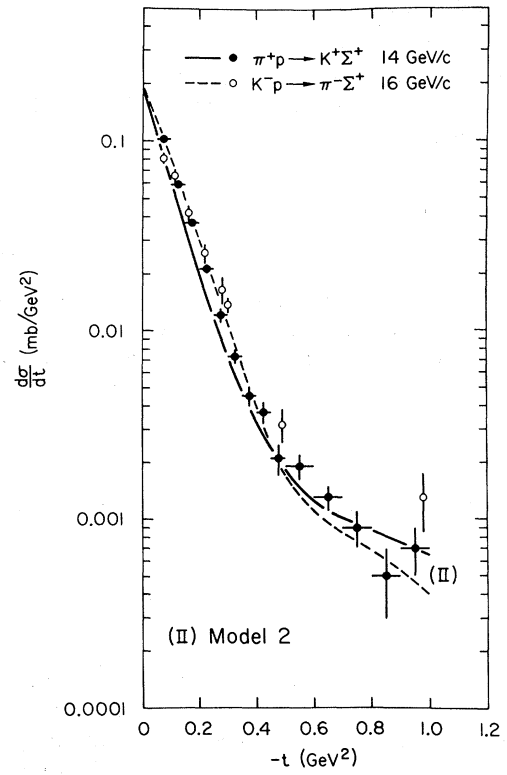

FIG. 15. Differential cross sections for $\pi^+p \rightarrow K^+\Sigma^+$ at 14 GeV/c (solid points), and for $K^-p \rightarrow \pi^-\Sigma^+$ at 16 GeV/c (open points). The solid (dashed) curves, denoted (II), are a comparison of the model 2 version of the DAM to πp ($\bar{K}p$) channels. The model comparisons have been calculated at 14 GeV/c.

K^{**} exchange amplitudes, we regard the results presented as a representative, but not unique, determination of the amplitudes. The parameters for the Σ data and the Λ data have been found separately and are summarized in Table V. The differential cross sections for model 1 are compared to the Σ reactions in Fig. 16 and to the Λ reactions in Fig. 17 over the momentum range ~4 to ~16 GeV/c. In Figs. 14 and 15 comparisons are made at specific energies for pairs of line-reversed reactions using both models 1 and 2. Good agreement is found with the differential-cross-section data; in particular, the model curves are able to describe simultaneously both the Σ reactions and the Λ reactions, even though these two sets of reactions behave quite differently under line reversal. The polarizations (see Figs. 12 and 13) are also adequately reproduced by the models. Thus both DAM parametrizations are found to provide good descriptions of all available data although somewhat better agreement is observed for model 2.

TABLE V. Model parameters for strangeness-exchange reactions.

Reaction	$K^-p \rightarrow \pi^-\Sigma^+$ Model 1	$K^-p \rightarrow \pi^-\Sigma^+$ Model 2	$\bar{K}^0p \rightarrow \pi^+\Lambda^0$ Model 1	$\bar{K}^0p \rightarrow \pi^+\Lambda^0$ Model 2
r (GeV^{-1})	5.04	4.97	4.77	5.13
$\Delta\alpha$	0.065	0.065	0.065	0.065
		K^* exchange		
A_V (GeV^{-2})	0.30	0.21	−0.17	−0.78
g_0^V	17.0	17.1	12.3	11.9
g_1^V	−18.5	−17.7	12.6	12.3
a_V (GeV^{-2})	3.23	3.61	0.79	2.51
b_V (GeV^{-4})	2.57	2.95	1.77	0.95
B_V (GeV^{-2})	0.0	0.0	0.0	0.0
x (GeV^{-2})	···	2.29	···	1.80
y (GeV^{-4})	···	2.01	···	0.82
		K^{**} exchange		
A_T (GeV^{-2})	−0.01	−0.17	−0.56	−0.69
g_0^T	2.95	2.48	2.36	2.31
g_1^T	−2.24	−2.41	2.26	2.97
a_T (GeV^{-2})	−0.77	−0.67	−0.48	−0.22
b_T (GeV^{-4})	−8.05	−7.87	−0.66	−6.15
B_T (GeV^{-2})	0.5	0.5	0.0	1.0

It is interesting to compare the results of the DAM analysis to the compilation of Λ and Σ slopes and forward differential cross sections. The results for the differential cross sections at $t=0$ are given in Figs. 8 and 10, and show the Regge dependence assumed in the model. In Figs. 9 and 11, two curves are displayed for each reaction corresponding to the model 2 slopes determined in the two momentum-transfer intervals, region A: ($0 \leq -t \leq 0.3$ GeV^2); and region B: ($0.1 \leq -t \leq 0.4$ GeV^2). The slope parameters are seen to differ considerably depending upon the t region chosen, especially for the πN induced channels where differences larger than 1 GeV^{-2} are found. These dependences on the t region may explain part of the scatter of the experimental slope values (see Fig. 9 and 11) and also may cause a spreading of the values for the forward differential cross sections that are determined by extrapolation. In particular, we note that for the πN channels the model yields a smaller slope for region B than for region A whereas the opposite is true for the $\bar{K}N$ channels. Extrapolation of these slopes would then yield

$$\frac{d\sigma/dt\,(\bar{K}N \rightarrow \pi Y)}{d\sigma/dt\,(\pi N \rightarrow KY)} > 1$$

at $t=0$ even if the true value of the ratio were unity. This trend is in fact suggested by the Σ data shown in Fig. 8.

The prediction for the S and T parameters for the Σ and Λ reactions are shown in Figs. 18 and 19, respectively. For the Σ data the two models are nearly indistinguishable, whereas for the Λ data the two models predict quite different t dependences. The measurements of the S and T parameters therefore would be essential in determining the true amplitude structure.

The s-channel helicity amplitudes, evaluated at 6 GeV/c, are shown in Figs. 20–23. The individual K^* and K^{**} amplitudes for the Σ reactions are essentially equal for the model 1 and 2 solutions (see Fig. 20), whereas for the Λ reactions the real parts of both the helicity-flip and -nonflip amplitudes differ appreciably between the model 1 and 2 solutions (see Fig. 21). As noted above, the S and T parameter predictions for the Λ data are correspondingly quite different for the two

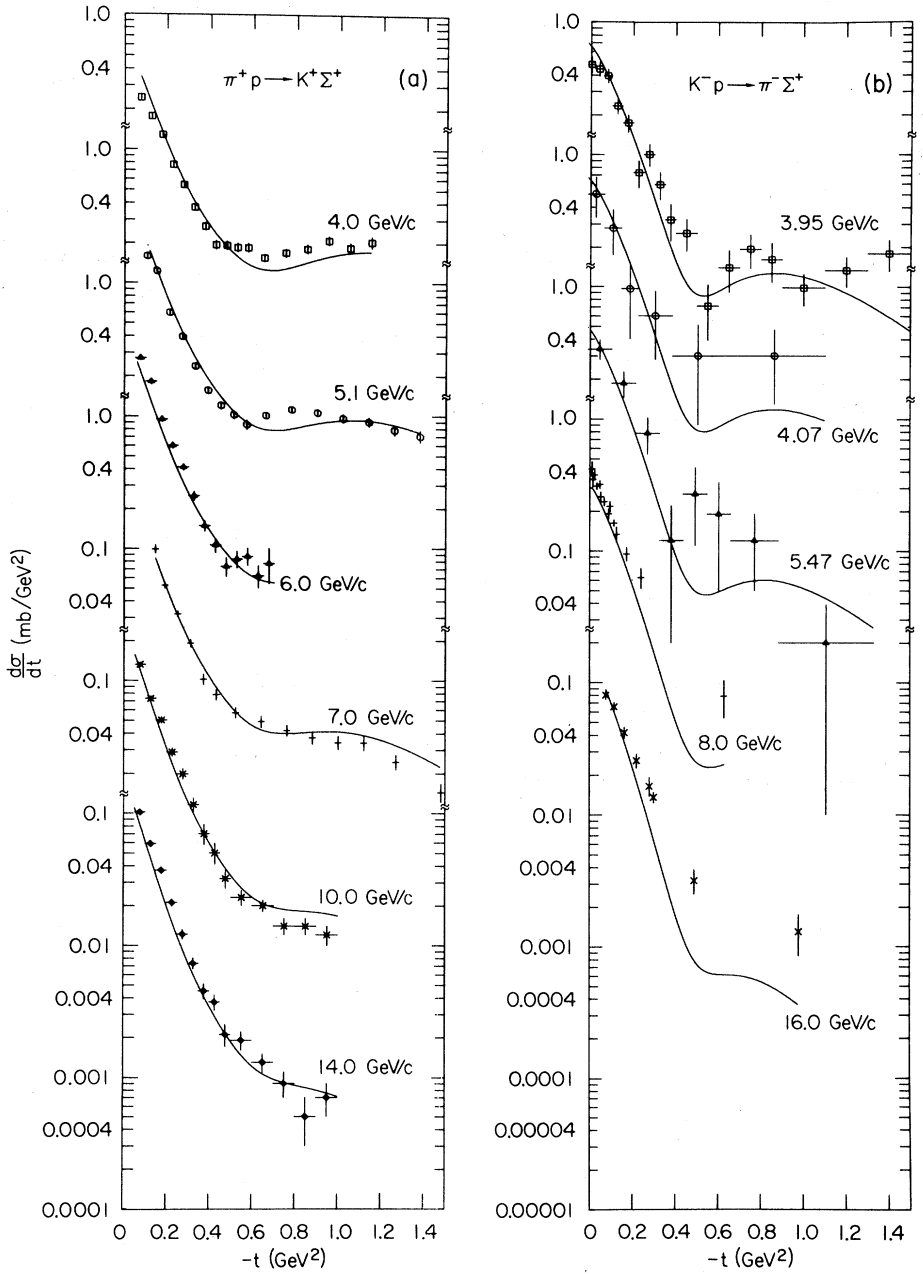

FIG. 16. Differential cross sections for (a) $\pi^+ p \rightarrow K^+ \Sigma^+$ and (b) $K^- p \rightarrow \pi^- \Sigma^+$ in the momentum interval ~4 to 16 GeV/c. The curves are a comparison of the DAM (model 1) to the data.

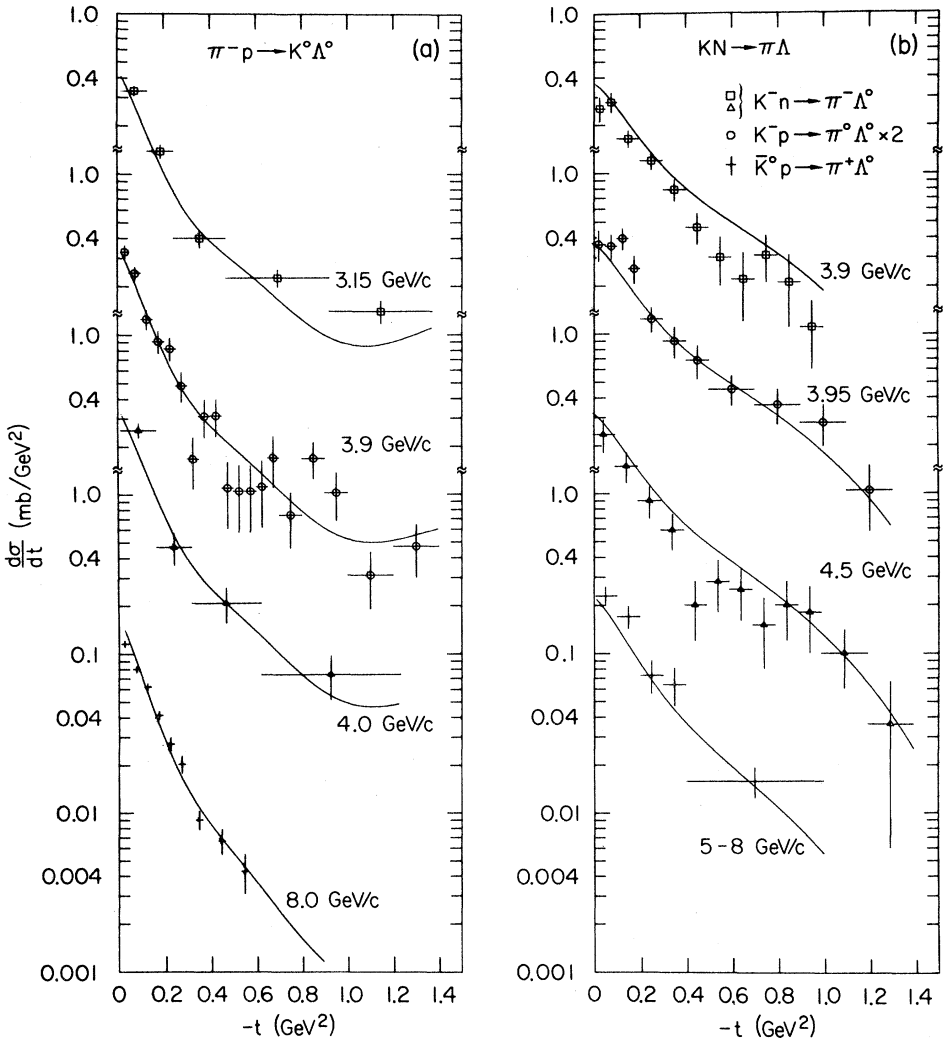

FIG. 17. Differential cross sections for (a) $\pi^- p \to K^0 \Lambda^0$ and (b) $\bar{K}N \to \pi\Lambda$ in the momentum interval ~ 3 to ~ 8 GeV/c. The curves are a comparison of the DAM (model 1) to the data.

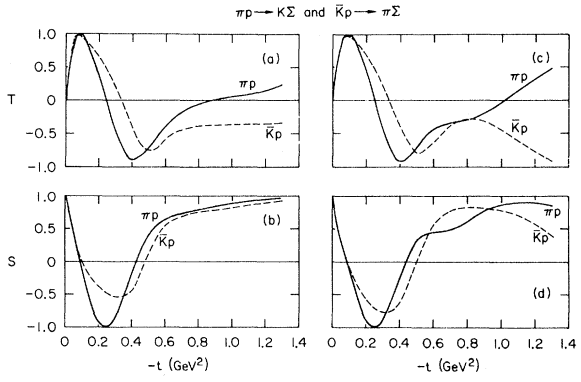

FIG. 18. Predictions of the DAM for (a) T and (b) S parameters for $\pi p \to K\Sigma$ (solid curve) and $\bar{K}p \to \pi\Sigma$ (dashed curve), respectively, as calculated from the DAM, model 1. Parts (c) and (d) are analogous, but are calculated from the DAM, model 2.

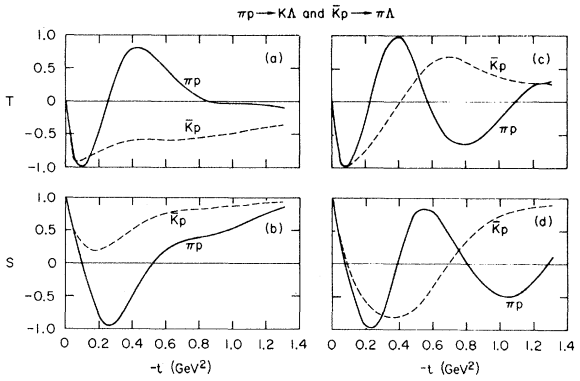

FIG. 19. Predictions of the DAM for (a) T and (b) S parameters for $\pi p \to K\Lambda$ (solid curve) and $\bar{K}p \to \pi\Lambda$ (dashed curve) as calculated from the DAM, model 1. Parts (c) and (d) are analogous, but are calculated from the DAM, model 2.

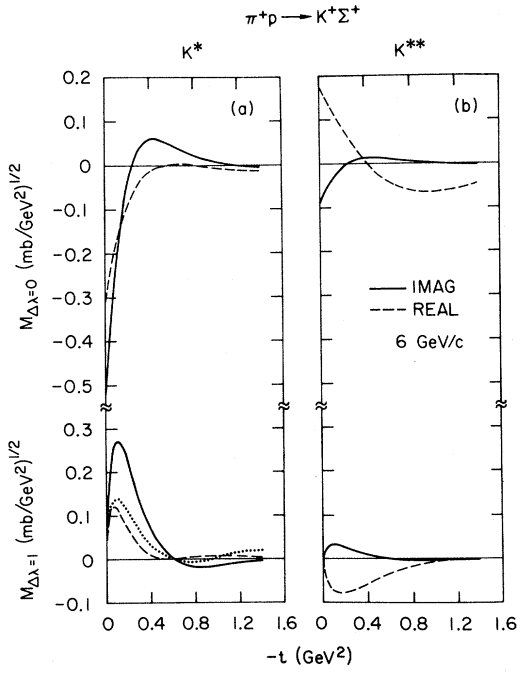

FIG. 20. s-channel helicity amplitudes for (a) K^* and (b) K^{**} exchanges in the channel $\pi^+p \rightarrow K^+\Sigma^+$ at 6 GeV/c. The solid (dashed) curves represent the imaginary (real) parts of the amplitudes. The curves are for the DAM, model 1, results. The DAM, model 2, results differ only in the real part of the K^* helicity-flip amplitude, which is shown as a dotted line in the figure.

models. The resultant amplitudes for specific Σ and Λ reactions are displayed in Figs. 22 and 23; the amplitudes for other strangeness-exchange reactions are simply related by Table III.

Several observations may now be made from the amplitudes determined in the present analysis:

(1) Qualitatively similar structures in momentum transfer are found for $\rho(A_2)$ and $K^*(K^{**})$ amplitudes using the model 2 results.

(2) For the Λ reactions the values for the exponential parameters, A, are in good agreement with the results for πN charge exchange and η production; however, somewhat different values are found for the Σ reactions.

(3) The approximate agreement with strong exchange degeneracy for the ρ and A_2 amplitudes in KN charge exchange is not found to apply to the K^* and K^{**} amplitudes in Σ and Λ production. Rather, the ratios of imaginary to real parts of the forward amplitudes for $\bar{K}p \rightarrow \pi(\Sigma, \Lambda)$ are observed to be approximately unity (see Figs. 22 and 23). In addition, from Table V we observe that the ratios of coupling constants are

$$|g^V(\Lambda)/g^T(\Lambda)| \simeq |g^V(\Sigma)/g^T(\Sigma)| \simeq 6,$$

for both helicity-flip and -nonflip amplitudes.[53] As noted previously, the failure of strong exchange degeneracy follows from our formulation of the DAM having equal radii of interaction for vector- and tensor-exchange amplitudes, and from the

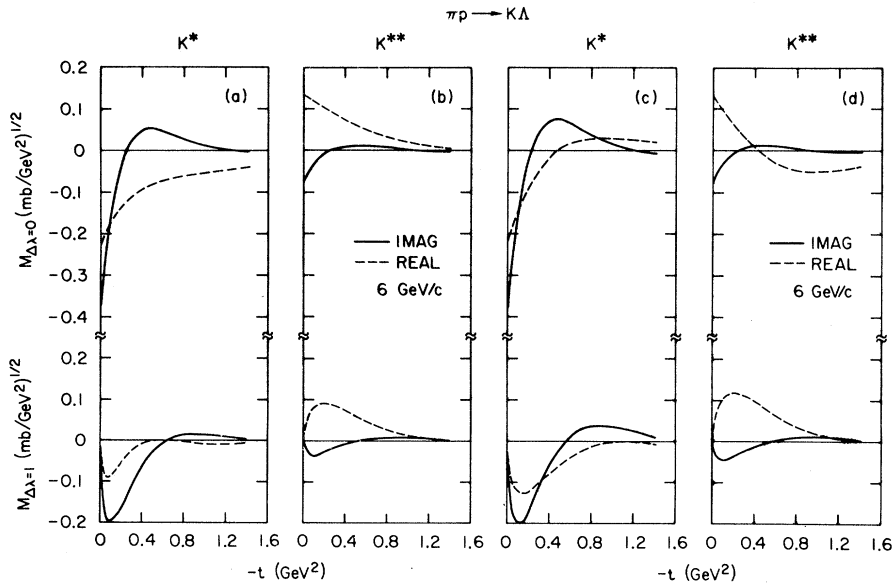

FIG. 21. s-channel helicity amplitudes for (a) K^* and (b) K^{**} exchanges in the channel $\pi^-p \rightarrow K^0\Lambda^0$ at 6 GeV/c. The solid (dashed) curves represent the imaginary (real) parts of the amplitude for the DAM, model 1, results. Parts (c) and (d) are the same as (a) and (b), respectively, but are for the DAM, model 2, results.

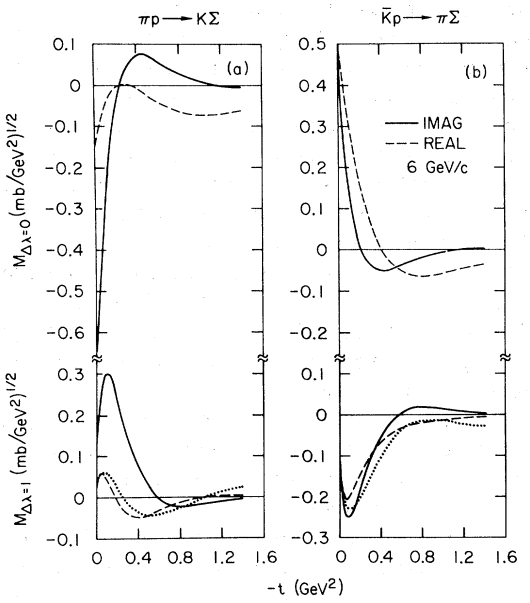

FIG. 22. Resultant s-channel helicity amplitudes, summed over K^* and K^{**} exchanges, for the reactions (a) $\pi^+p \to K^+\Sigma^+$ and (b) $K^-p \to \pi^-\Sigma^+$ at 6 GeV/c. The solid and dashed curves represent the imaginary and real parts of the amplitudes, respectively. Amplitudes for other channels are related as given in Table III. The curves show the DAM, model 1, results. The DAM, model 2, results only differ in the real parts of the helicity-flip amplitudes, which are shown as a dotted curve in the figure.

large polarization observed in the $\bar{K}N$ strangeness-exchange data.

(4) The apparent failure of strong exchange degeneracy for K^* and K^{**} amplitudes implies a breaking of SU(3) symmetry. That is, the K^* and K^{**} amplitudes are not directly related by SU(3) scalar coefficients to the ρ and A_2 amplitudes determined in the analysis of reactions (1)–(4). Furthermore, if the coupling constants for the (Λ, Σ) reactions are compared to those for the KN charge-exchange reactions, then the f/d ratios found are incompatible with those determined for the (ρ, ω^0) exchanges (see Table IV). It is interesting to note, however, that if the coupling constants for the Σ reactions are compared to those for the Λ reactions then f/d ratios are derived which are in good agreement with those found for the (ρ, ω^0) exchanges.

IV. SUMMARY AND CONCLUSIONS

The present analysis shows that a consistent description of pseudoscalar-meson–baryon scattering can be achieved within the amplitude framework of the dual absorptive model (DAM). The amplitudes determined in the present study reproduce well the data for reactions (1)–(6) and also satisfy the requirements imposed by previous amplitude analyses of elastic scattering data. The hypothesis of strong exchange degeneracy is found to be approximately satisfied for (ρ, A_2) exchange

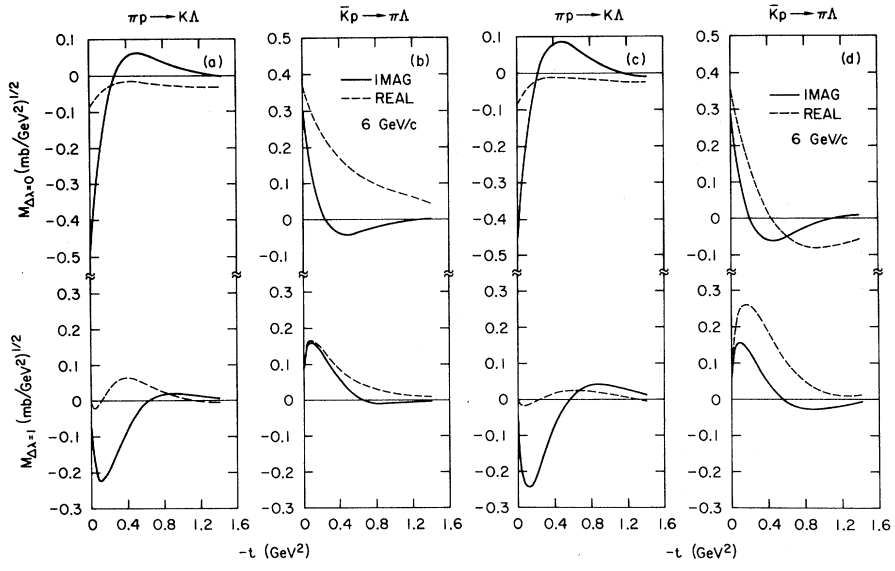

FIG. 23. Resultant s-channel helicity amplitudes, summed over K^* and K^{**} exchanges, for the reactions (a) $\pi^-p \to K^0\Lambda^0$ and (b) $\bar{K}^0p \to \pi^+\Lambda^0$ at 6 GeV/c. The solid and dashed curves represent the imaginary and real parts of the amplitudes respectively. Amplitudes for other channels are related as shown in Table III. The curves show the DAM, model 1, results. Parts (c) and (d) are same as (a) and (b), respectively, but show the DAM, model 2, results.

in $K^-p \to \bar{K}^0 n$ and $K^+ n \to K^0 p$ (where the s channel is exotic for the $K^+ n$ case), but is significantly violated for (K^*, K^{**}) exchange in the reactions $\pi N \to KY$ and $\bar{K}N \to \pi Y$ (where the s channel is not exotic for either reaction).

The reactions (1)–(4) are closely related since they involve nonstrange vector (ρ, ω^0) and tensor (A_2) meson exchanges with exchange-degenerate Regge trajectories. The model satisfactorily describes the available data on these reactions, except perhaps for the $K_L^0 p \to K_S^0 p$ data for $-t \gtrsim 0.3$ GeV^2.

The ρ-amplitude structure determined in the present work, where

$$\mathrm{Im}M_{\Delta\lambda} \propto J_{\Delta\lambda}(r\sqrt{-t})e^{At},$$

is observed to be consistent with the results of previous amplitude analyses. Essentially equal values for the parameters r (radius of interaction) and A are found for the ρ and A_2 amplitudes (predominantly $\Delta\lambda = 1$); these values also are in agreement with the parameters obtained for $(\rho, \omega)^0$ and f^0 exchanges from elastic scattering data (predominantly $\Delta\lambda = 0$). This result suggests that the impact-parameter representations for all of these exchange amplitudes are approximately equal.

The comparison of the ρ and A_2 amplitudes to KN charge-exchange data yields coupling constants which are in good agreement with SU(3) predictions. The resulting amplitudes for $K^+ n \to K^0 p$ are approximately real, and the polarization for this reaction is expected to be small. This result suggests that strong exchange degeneracy applies to absorbed Regge-exchange amplitudes in exotic channels.

The vector couplings determined for $\pi^- p \to \pi^0 n$ and $K_L^0 p \to K_S^0 p$ yield SU(3) f/d ratio values $(f/d)_{\Delta\lambda=0} \sim -5.3$ and $(f/d)_{\Delta\lambda=1} \sim 0.32$ in good agreement with previous studies.

We have summarized the data for the reactions $\pi N \to KY$ and $\bar{K}N \to \pi Y$, where Y is Λ^0 or Σ, by compiling the differential cross sections at $t = 0$, $(d\sigma/dt)_0$, and the slopes of the forward differential cross section, B, in the momentum interval ~3 to ~16 GeV/c. The data are observed to satisfy the following relations:

$$\left(\frac{d\sigma}{dt}\right)_0 (\pi N \to KY) \simeq \left(\frac{d\sigma}{dt}\right)_0 (\bar{K}N \to \pi Y)$$

and

$$B(\pi N \to KY) > B(\bar{K}N \to \pi Y),$$

where the inequality of the slope parameter is especially pronounced for the Λ^0 reactions. The equality of the forward cross sections suggests that the Regge phases hold at $t = 0$ $[\alpha_{K^*}(0) \simeq \alpha_{K^{**}}(0)]$, and that absorption does not alter the phases of the forward amplitudes appreciably. This result is supported by πN charge exchange and also K_S^0 regeneration data where the experimentally determined phases are near the values predicted by Regge theory. However, absorption does alter the amplitudes significantly for $-t > 0$ and can cause the observed differences in the slopes of the forward cross sections for line-reversed pairs of reactions.

The polarization data for the strangeness-exchange reactions are also compiled in the momentum interval ~4 to ~14 GeV/c. Polarizations for both πN and $\bar{K}N$ channels are observed to be large, to be nearly independent of energy, and to be satisfied approximately by the relations: $P(\pi N \to K\Lambda) = -P(\pi N \to K\Sigma)$ and $P(\bar{K}N \to \pi\Lambda) = -P(\bar{K}N \to \pi\Sigma)$. The large values of polarization are in disagreement with the expectations of the duality diagrams for strong exchange degeneracy in $\bar{K}N$ channels.

The present analysis reproduces well the observed features of the strangeness-exchange reactions (5) and (6), using the same basic amplitude structure for K^* and K^{**} exchanges as for ρ and A_2 exchanges. However, the relation between coupling constants for the (ρ, A_2)-exchange reactions and the (K^*, K^{**})-exchange reactions indicates that the K^{**} is suppressed with respect to K^* in disagreement with SU(3) predictions. In the present formulation of the DAM, where nearly equal radii of interaction are used for vector and tensor exchanges, the suppression of K^{**} relative to K^* is needed in order to reproduce the large polarization observed in reactions (5) and (6). The K^*/K^{**} ratio of couplings suggests that one should be cautious about applying SU(3) symmetry between the (K^*, K^{**}) and (ρ, A_2) exchanges.

In conclusion, the present formulation of the DAM provides a consistent picture of inelastic pseudoscalar-meson–baryon scattering. In order to evaluate the validity of the amplitudes determined in the present analysis, further experimental work is necessary. Measurements which appear to be particularly needed for further progress are: (1) polarization for $\pi^- p \to \eta^0 n$ for $-t > 0.2$ GeV^2, (2) $d\sigma/dt$ for $\bar{K}N \to \pi\Lambda^0$, (3) polarization for $\bar{K}N \to \pi\Lambda^0$ and $\bar{K}N \to \pi\Sigma$ above ~8 GeV/c, and the more difficult measurements of (4) polarization in $K^+ n \to K^0 p$, and (5) S and T parameters in strangeness-exchange reactions.

ACKNOWLEDGMENTS

We would like to thank Y. Avni and F. Gilman for critical readings of the manuscript, M. Davier and R. Cashmore for stimulating discussions, and

D. Leith for his support and interest. We also wish to acknowledge the private communication of data in advance of publication by R. Yamartino, C. Ward, D. Reeder, J. Lynch, W. Love, and R. Eisner.

---

*Work supported by the U. S. Atomic Energy Commission.

[1]V. Barger and R. J. N. Phillips, Phys. Rev. 187, 2210 (1969); Phys. Rev. Letters 21, 865 (1968); A. Ahmadzadeh and W. B. Kaufmann, Phys. Rev. 188, 2438 (1969); T. J. Gajdicar, R. K. Logan, and J. W. Moffat, *ibid.* 170, 1599 (1968); D. D. Reeder and K. V. L. Sarma, *ibid.* 172, 1566 (1968).

[2]A. D. Martin, C. Michael, and R. J. N. Phillips, Nucl. Phys. B43, 13 (1972).

[3]C. Schmid and J. K. Storrow, Nucl. Phys. B29, 219 (1971); G. V. Dass, J. Frøyland, F. Halzen, A. Martin, C. Michael, and S. M. Roy, Phys. Letters 36B, 329 (1971).

[4]R. J. N. Phillips and G. A. Ringland, Nucl. Phys. B32, 131 (1971).

[5]G. I. Ghandour and R. G. Moorhouse, Phys. Rev. D 6, 856 (1972); R. D. Field and J. D. Jackson, *ibid.* 4, 693 (1971); F. J. Gilman, H. Harari, and Y. Zarmi, Phys. Rev. Letters 21, 323 (1968); H. Harari and Y. Zarmi, Phys. Rev. 187, 2230 (1969); A. C. Hirshfeld, Phys. Letters 39B, 233 (1972).

[6]N. Barik, B. P. Desai, P. Kaus, and R. T. Park, Phys. Rev. D 4, 2923 (1971); B. P. Desai, P. Kaus, R. T. Park, and F. Zachariasen, Phys. Rev. Letters 25, 1389 (1970); D. P. Roy, J. Kwiecinski, B. P. Desai, and F. Zachariasen, Phys. Letters 34B, 512 (1971); P. Chýlek, Phys. Rev. D 4, 3509 (1971).

[7]A. Martin and P. R. Stevens, Phys. Rev. D 5, 147 (1972).

[8]J. P. de Brion, A. Derem, and J. Dronkers, Nucl. Phys. B32, 557 (1971).

[9]J. W. Coleman and R. C. Johnson, Nucl. Phys. B33, 614 (1971).

[10]G. A. Ringland, R. G. Roberts, D. P. Roy, and J. Tran Thanh Van, Nucl. Phys. B44, 395 (1972).

[11]F. Henyey, G. L. Kane, J. Pumplin, and M. H. Ross, Phys. Rev. 182, 1579 (1969).

[12]R. C. Arnold and M. L. Blackmon, Phys. Rev. 176, 2082 (1968).

[13]M. L. Blackmon and G. R. Goldstein, Phys. Rev. 179, 1480 (1969).

[14]A. C. Irving, A. D. Martin, and C. Michael, Nucl. Phys. B32, 1 (1971).

[15]R. D. Field, Phys. Rev. D 5, 86 (1972).

[16]A. Krzywicki and J. Tran Thanh Van, Phys. Letters 30B, 185 (1969).

[17]C. Meyers, Y. Noirot, M. Rimplaut, and Ph. Salin, Nucl. Phys. B23, 99 (1970).

[18]F. Halzen and C. Michael, Phys. Letters 36B, 367 (1971).

[19]G. A. Ringland and D. P. Roy, Phys. Letters 36B, 110 (1971).

[20]V. Barger and A. D. Martin, Phys. Letters 39B, 379 (1972).

[21]F. Hayot and H. Navelet, Phys. Letters 37B, 424 (1971).

[22]G. Höhler and R. Strauss, Karlsruhe report, 1971 (unpublished).

[23]H. Harari, Ann. Phys. (N.Y.) 63, 432 (1971).

[24]R. Dolen, D. Horn, and C. Schmid, Phys. Rev. 168, 1766 (1968); M. Fukugita, T. Inami, and Y. Kimura, Phys. Letters 36B, 575 (1971).

[25]H. Harari, SLAC Report No. SLAC-PUB-914 (unpublished).

[26]H. Harari, Phys. Rev. Letters 22, 562 (1969); J. L. Rosner, *ibid.* 22, 689 (1969).

[27]H. Harari, Phys. Rev. Letters 20, 1395 (1968); P. G. O. Freund, *ibid.* 20, 235 (1968).

[28]H. Harari, Phys. Rev. Letters 26, 1400 (1971).

[29]M. Davier and H. Harari, Phys. Letters 35B, 239 (1971).

[30]D. Cline and J. Matos, Nucl. Phys. B33, 421 (1971).

[31]H. A. Gordon, K.-W. Lai, and F. E. Paige, Phys. Rev. D 5, 1113 (1972); M. Davier, Phys. Letters 40B, 369 (1972).

[32]R. C. Arnold, Phys. Rev. Letters 14, 657 (1965); J. D. Jackson, Rev. Mod. Phys. 42, 12 (1970).

[33]K.-W. Lai and J. Louie, Nucl. Phys. B19, 205 (1970).

[34]F. J. Gilman, Phys. Letters 29B, 673 (1969); D. Cline, J. Matos, and D. D. Reeder, Phys. Rev. Letters 23, 1318 (1969); R. D. Matthews, Nucl. Phys. B11, 339 (1969).

[35]H. Harari and A. Schwimmer, Phys. Rev. D 5, 2780 (1972).

[36]For the real parts of the helicity-nonflip amplitudes, the polynomial describes the approximate zero structure while the exponential parameter, B, provides damping of the polynomial term with increasingly negative momentum transfers. Only the πN charge-exchange data was sufficiently precise to evaluate the polynomial parameter c_V; for all other reactions c_V was set to zero.

[37]W. B. Johnson, D. W. G. S. Leith, J. S. Loos, G. J. Luste, K. Moriyasu, W. M. Smart, F. C. Winkelmann, and R. J. Yamartino, Phys. Rev. Letters 26, 1053 (1971); P. Darriulat, G. Grosso, M. Holder, J. Pilcher, E. Radermacher, C. Rubbia, M. Scire, A. Staude, and K. Tittel, Phys. Letters 33B, 433 (1970); C. D. Buchanan, D. J. Drickey, F. D. Rudnick, P. F. Shepard, D. H. Stork, H. K. Ticho, C. Y. Chien, B. Cox, L. Ettlinger, L. Resvanis, R. A. Zdanis, E. Dally, E. Seppi, and P. Innocenti, *ibid.* 37B, 213 (1971); V. K. Birulev *et al.*, *ibid.* 38B, 452 (1972).

[38]For $r = 5$ GeV^{-1}, $\beta(t') = 0.43 + 0.72t'$, which then closely resembles the ρ Regge trajectory, $\alpha(t) = 0.5 + 0.9t$.

[39]A slow energy dependence to some of the parameters will not significantly alter the present results. We note that the present model with Regge shrinkage and fixed interaction radius will yield a nonperipheral amplitude at very large energies (Ref. 35). Also, in principle some energy dependence of the parameters is needed to generate a non-Regge phase in the $\Delta\lambda = 0$ amplitudes (Ref. 35).

[40]When the amplitude structure is explicitly plotted in this paper (Figs. 4, 6, 20–23) we show the quantity $(\hbar c/8q\sqrt{\pi s})M_{\Delta\lambda}$ in units of mb$^{1/2}$/GeV.

[41]E. L. Berger and G. Fox, Phys. Rev. Letters 25, 1783 (1970); R. J. Cashmore and A. J. G. Hey, Phys. Rev. D 6,

1303 (1972).

[42]A comparison of the amplitudes to only the differential cross section cannot distinguish the sign of $\mathrm{Re}M_{\Delta\lambda=0}$ for $-t>0.2$ GeV^2 between the present solution, Fig. 4(b), and a solution similar to the ρ amplitude, Fig. 4(a). If the η^0 polarization is calculated assuming $\mathrm{Re}M_{\Delta\lambda=0}<0$ for $-t<1.0$ GeV^2, the resulting polarization prediction is qualitatively similar to the curve in Fig. 3 but has a smaller magnitude in the region $-t>0.4$ GeV^2.

[43]At 5 GeV/c, typical values of A' and r are 1.3 GeV^{-2} and 5 GeV^{-1}, respectively. With these parameters the difference between $\Delta\lambda=0$ and $\Delta\lambda=1$ amplitudes is then $<10\%$ for $b>2.6$ GeV^{-1} ($\sim\frac{1}{2}$ fm).

[44]A. Firestone, G. Goldhaber, A. Hirata, D. Lissauer, and G. H. Trilling, Phys. Rev. Letters 25, 958 (1970).

[45]F. J. Gilman, Phys. Rev. 171, 1453 (1968).

[46]Wherever possible the quantities shown in Figs. 8–11 are taken from data in the region $0.0\lesssim -t\lesssim 0.4$ GeV^2. For the reaction $\bar{K}N\to\pi\Lambda$, there is no clear break in the differential cross section, and slopes were accepted when calculated over a large momentum-transfer range.

[47]For example, see Table III where it is seen that an appropriate choice of SU(3) f/d ratios could account for the observed mirror symmetry.

[48]In Σ production isospin-$\frac{3}{2}$ states can also contribute in the t channel. Such exchanges are exotic, and are expected to decrease in importance very rapidly with energy. Experimental tests made above 3 GeV/c indicate predominance of isospin $\frac{1}{2}$ in the t channel [see D. J. Crennell, H. A. Gordon, K. W. Lai, and J. M. Scarr, Phys. Rev. D 6, 1220 (1972); L. Moscoso, J. R. Hubbard, A. Laveque, J. P. de Brion, C. Louedec, D. Revel, J. Badier, E. Barrelet, A. Rouge, H. Videau, and I. Videau, Nucl. Phys. B36, 332 (1972)].

[49]M. Ferro-Luzzi, H. K. Shepard, A. Vernan, R. T. Poe, and B. C. Shen, Phys. Letters 34B, 524 (1971); A. Kernan, R. T. Poe, B. C. Shen, I. Butterworth, M. Ferro-Luzzi, and H. K. Shepard, U. C. Riverside report, 1972 (unpublished).

[50]A recent analysis (Ref. 20) of the Σ and Λ reactions does assume strong exchange degeneracy for the helicity-flip amplitudes and consequently implies either nonperipheral imaginary parts for the nonflip amplitudes, or substantially different radii of interaction for K^* and K^{**} amplitudes.

[51]A. Bashian, G. Finocchiaro, M. L. Good, P. D. Grannis, O. Guisan, J. Kirz, Y. Y. Lee, R. Pittman, G. C. Fischer, and D. D. Reeder, Phys. Rev. D 4, 2667 (1971).

[52]In separate comparisons of the DAM amplitudes to the Σ and Λ data values were obtained of $\Delta\alpha=0.12$ and $\Delta\alpha=0.01$, respectively. For the comparisons tabulated in Table V and shown in the figures the parameter $\Delta\alpha$ was fixed to the average of the Σ and Λ results to simplify the evaluation of SU(3) f/d factors. We have used $\alpha(t)=0.5+0.9t$ and $\alpha_V(0)=0.33$.

[53]We note that the precise values of these ratios are significantly correlated to the choice for the phase of the amplitudes at $t=0$, which unfortunately is only poorly determined by the present data. This correlation is mainly due to the approximate equality, $\mathrm{Re}A_V\simeq\mathrm{Re}A_T$ [see discussion following Eq. (16)], which implies the following ratio for K^* and K^{**} coupling constants [see Eqs. (8), (9), and (17)]: $g^V/g^T\sim\cot[\frac{1}{2}\pi\alpha_V(0)]^2$. This ratio is ~ 3 for the K^* trajectory intercept, $\alpha_V(0)=0.33$, used in the present analysis. However, if we choose the ρ Regge intercept, $\alpha_V(0)=0.5$, we then find the ratio $g^V/g^T\sim 1$ and the ratio $\mathrm{Im}M_{\Delta\lambda=0}/\mathrm{Re}M_{\Delta\lambda=0}\sim 0.4$ for both Σ and Λ channels. The amplitudes resulting from the use of the ρ Regge phase yield polarization and differential cross-section predictions that cannot be excluded by the present data.

PHYSICAL REVIEW D VOLUME 6, NUMBER 9 1 NOVEMBER 1972

Low-Energy Theorems and High-Energy Behavior*

Michael Creutz
Center for Theoretical Physics, Department of Physics and Astronomy, University of Maryland, College Park, Maryland 20742

(Received 17 April 1972)

We study the constraints at high energy that analyticity imposes on amplitudes given a low-energy theorem and an upper bound to the amplitude at intermediate energies. These constraints prove to be nontrivial when applied to the pion electromagnetic form factor. We suggest that our results may be useful in a future analysis of the contribution of the spin-dependent forward Compton amplitude to unpolarized Compton scattering. This application will require experimental data on the forward differential cross section in the resonance region.

In a recent paper Levin, Mathur, and Okubo [1] have phenomenologically discussed bounds on the pion charge radius in terms of the modulus of the pion electromagnetic form factor on its cut. In this analysis they discovered an interesting side result. They found that the modulus of the pion form factor cannot begin to fall rapidly in a "dipole" fashion until a four-momentum transfer squared of at least 17 GeV^2 is reached. What is remarkable about this result is the small amount